AN APPROACH TO ANALYZING HISTOLOGY SEGMENTATIONS USING SHAPE DISTRIBUTIONS

A Thesis

Submitted to the Faculty

of

Drexel University

by

Jasper Z. Zhang

in partial fulfillment of the

requirements for the degree

of

Master of Science

in

Computer Science

March 2008

ACKNOWLEDGMENTS

The U.S. Army Medical Research Acquisition Activity, 820 Chandler Street, Fort Detrick, MD 21702-5014 is the awarding and administering acquisition office. This investigation was partially funded under a U.S. Army Medical Research Acquisition Activity; Cooperative Agreement W81XWH 04-1-0419.

The content of the information herein does not necessarily reflect the position or the policy of the U.S. Government, the U.S. Army or Drexel University and no official endorsement should be inferred. Any opinions, findings, and conclusions or recommendations expressed in this material are those of the author.

TABLE OF CONTENTS

LIST OF TABLES

Number *Page*

LIST OF FIGURES

Number *Page*

LIST OF EQUATIONS

Number *Page*

ABSTRACT

AN APPROACH TO ANALYZING HISTOLOGY SEGMENTATIONS USING SHAPE DISTRIBUTIONS

Jasper Zhang

David E. Breen, Ph. D.

Histological images are the key ingredients in medical diagnosis and prognosis in today's medical field. They are imagery acquired by analysts from microscopy to determine the cellular structure and composition of a patient's biopsy. This thesis provides an approach to analyze the histological segmentation obtained from histological images using shape distributions and provides a computationally feasible method to predict their histological grade.

This process provides a way of generating suggestions using segmented images in a way that is independent of the segmentation process. The process generates histograms for each image that describes a set of shape distributions generated from eight metrics that we have devised. The shape distributions are extracted from a learning set that the user provides. The shape distributions are then analyzed by querying a classification for each case using K-nearest-neighbor. The quality of the classifications is measured by a composite measure composed of precision and recall based on the query.

Chapter 1

INTRODUCTION

Computational histology is a new and emerging field in medical imaging in today's world and for a good reason. The demand for histological analysis is becoming increasingly large while the number of providers of such a service has stayed about the same [54] [3]. To cope with this increasing problem of consumer vs. producer, more and more pathologists have turned to automating their work through computational histology [53]. But as research has shown, it is not easy to extract meaningful information from a histological slide [7]. This paper proposes a way to acquire information from a histological segmentation and suggest histological grading for new cases.

1.1 Pathology and histology

Pathology (also known as pathobiology), under the definition of American Heritage Science Dictionary, is "the scientific study of the nature of disease and its causes, processes, development, and consequences." What that means for the everyday person is that pathologists are the people that can definitively say what disease, if any, we have and what the diagnosis and prognosis of the disease are. The pathologist is one of the crucial specialists in treating a patient who has a disease.

Though it is not always like this, the process of patient care can be generalized into Figure 1-1.

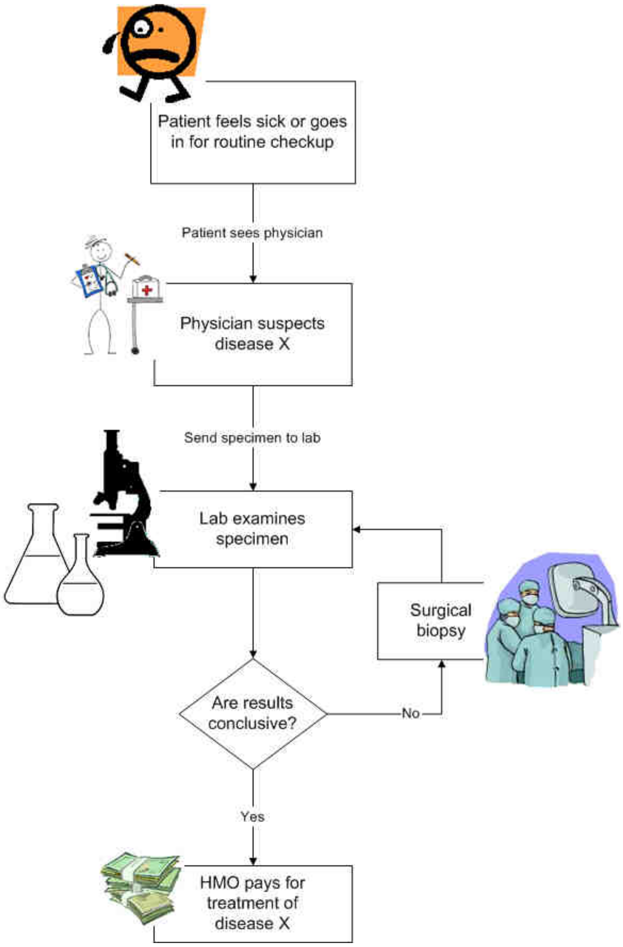

Figure 1-1 Medical process

As we can see from the diagram, a pathologist doesn't come into the picture in the lab process until after a biopsy or sample of the patient is extracted. This means the pathologist is only dealing with samples of the patient, not inferring anything from just symptoms. So what this brings up is that pathologists are really dealing with histology when they do their job. Histology, under the definition of American Heritage Science Dictionary, is "the branch of biology that studies the microscopic structure of animal or plant tissues." This definition allows for some development on the computational front mainly due to the key phrase "microscopic structure". What that implies is that it is a study of the shapes and geometry of an image. This is what allows us to consider our work in this thesis.

The information that a pathologist gains from a histological study allows them to generate diagnosis and prognosis for the patient. This diagnosis can fall under many different histological grades. The histological grades are determined by an existing heuristic specifically designed for the disease and allow the pathologist to easily come up with a diagnosis that is fitting for the patient.

1.2 Shape distribution

The main objective of this thesis is to develop a computational method that is capable of discriminating between histological images based on their geometry. This objective can only be achieved by giving each image a set of metrics that allows them to be compared. The obvious problem of this operation is the comparison itself. How can you compare a dataset, such as an image, with another in a meaningful way? Shape distribution gives a suitable solution to this problem. A shape distribution is a signature of the image in a fashion that allows for quantitative comparisons.

A shape distribution of an image is a sample of that image based on the application of a shape function that measures the local geometric properties and captures some global statistical property of an object. What this means is that the shape distributions will represent the image in a way that describes the statistical occurrences resulting from a shape function. That shape function can be anything; it can be passing a line through the image, how likely you are to sample a certain color when a random pixel is picked, how big each area of certain criteria is, etc.

The objective of this thesis is to build shape functions (that we call metrics) that can generate shape distributions that can aid in classifying histological segmentations. The helpfulness or success of a shape function is described by how well it can identify similar shapes as similar and how well it can identify dissimilar shapes as dissimilar while all at the same time be able to operate independently of any reorientation and repositioning that can happen to the image [42].

1.3 Previous work

Most of the work done in this area in the past has been focused mostly on segmentation. A majority of the reason why it hasn't moved on is based on the fact that biological images are still a challenge to segment. It is one of the hardest problems facing computer vision and image analysis to this day [34]. Part of the reason is that due to the over abundance of information it is hard to segment images from medical domain to medical domain using the same process [31] [43]. Many ad hoc techniques were developed for problem specific application to overcome this problem [7] [41] [45].

Due to the problem of segmenting the images many experts have used information on geometry and other analysis-based information to help segment the image [56] [14]. This leads to a hybrid approach between analysis and segmentation that has both happening at the same time. This leads to a solution to analysis and segmentation at the end of the whole process. This approach, too, is limited to a specific problem domain.

In recent years many experts have given up on trying to fully automate segmentation and reverted to using only semi-automatic techniques [40] [37] [38] [19] [33]. These techniques involve having human intervention as well as a mix of techniques stated above. Thought these techniques involve human intervention, they will almost always guarantee a satisfactory result for the user, at least in areas that the user is concerned with. This approach introduces a new problem of human computer interaction with the need of a well defined user interface that is easy and fast to use [36] [46].

The topic of segmentation is already hard to work with, as we have seen, which leads to the sparse field of segmentation analysis. A majority of this work has been done in conjunction with segmentation, as stated earlier, but there are some works that have been done on segmentations only [16] [32]. The results of the studies are very data-centric. The analysis themselves can only be as good as the segmentations themselves.

1.4 Our goal

The ultimate goal in this research is to create a process that can take, as inputs, segmentations of histological images and output a suggested histological grade of an unknown case. The classifications will be defined by the user by giving the system a learning set. The specific histological grade outputted by the system is based on the Nottingham scoring system.

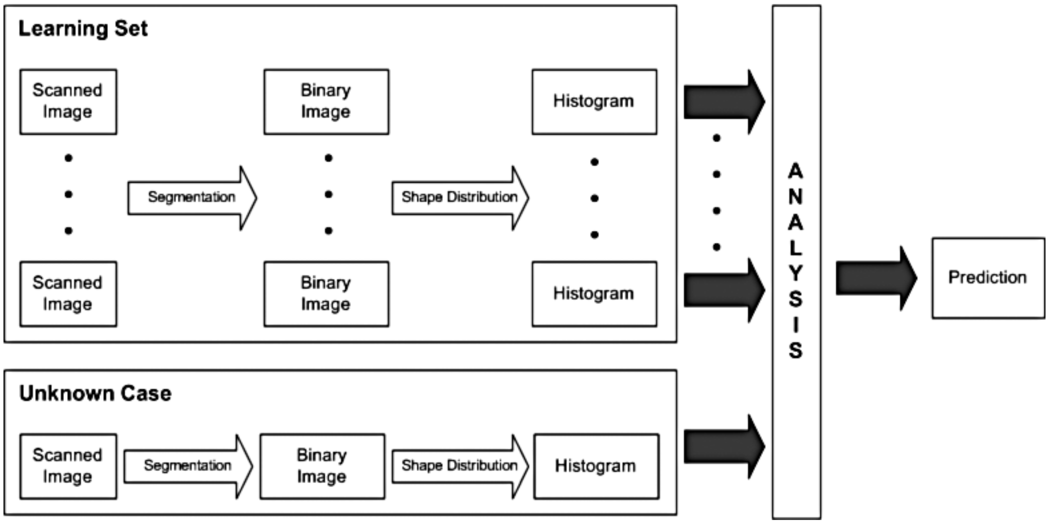

Figure 1-2 A broad overview of the computational pipeline.

This research also explores the usefulness of specific shape functions when applied to histology segmentations. Even if we don't achieve the ultimate goal of suggesting histological grade, we would like to at least be able to state a quantitative success of a given shape function with the given histology segmentations.

1.5 Our process

The work in this thesis falls under the last category in the previous work section. Our process generates analysis based on segmentations, not analysis parallel to segmentation. The overall process that we propose is shown in Figure 1-2. This process takes in a learning set to define classification groups and an unknown case or set of unknown cases whose histological grade will be predicted. What this process involves is to first digitize the slides into digital images. The digital images are then segmented to produce binary images that represent only the background and the areas of interest. The binary images are then transformed into histograms that represent the shape distribution produced by applying geometric measures to the images. The distributions are then analyzed and used to suggest the classification of the unknown cases.

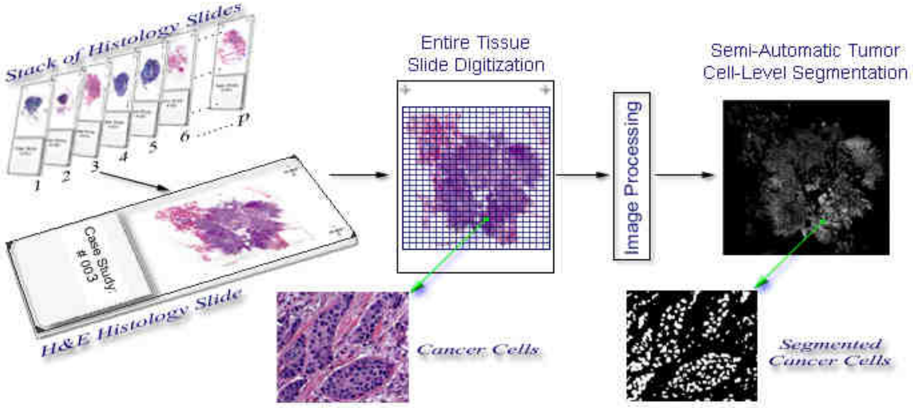

Figure 1-3 Segmentation process

The first stage of the pipeline is the digitization of the slides (Figure 1-3). The slides are given to us as a set of Hematoxylin and Eosion (H&E) stained slides. The slides are then scanned one sub-region at a time to ensure maximum detail and resolution. The individual images are then stitched together into a single large image that represents the slide.

The next stage in the process is the segmentation stage where the raw image is taken and a binary image will be the output. The process will first take an image and convert it into our optimal color space and a user interface will guide the user in helping the system determine the proper segmentation of the image. The user "trains" the system based on the definition of cells, as we are only interested in studying the morphology of cells within our slides in this study.

Once a binary image has been segmented out of the original H&E image, we are ready to convert it into shape distributions. The shape distributions are digital signatures that are produced by the computational pipeline when the geometric measures are applied to the segmentations. Several metrics will be used to generate multiple histograms per image for both the learning set and the unknown cases.

Our final stage is the analysis stage where we take our learning set's histograms and form classification groups that may be used to classify any unknown cases using the unknown cases' histograms. The result of this stage will be purely based on the segmentations.

1.6 Thesis structure

This thesis is structured into five chapters. This first chapter gives an introduction to the topic covered in this thesis. The second chapter will discuss the overall computational pipeline with specific emphasis on the generation of the shape distributions. The third chapter is dedicated to the processing of the segmentations prior to the generation of shape distributions and the filtering of the shape distributions before the analysis. The fourth chapter outlines our approach to analyzing the shape distributions after all the filtering described in chapter three have been applied. The final chapter makes a few final remarks on our work.

Chapter 2

COMPUTATIONAL PIPELINE

The computational pipeline that we are working with starts with a scanned section of a biopsy. We make no assumptions about the color corrections or the magnifications of the image when it is first presented. We assume the user to be the responsible party for assuring data coherency.

The input data must be segregated into two groups: the learning set and the unknown case(s). The learning set will also need to be segregated into classification groups. The classification groups will determine the set of all possible categories into which an unknown case can be placed. The pipeline will not take into account all subcategories that may exist within a group. If subcategories do exist within a group then the user must define them as separate classification groups.

The user must also take into consideration at scale of which images were scanned before processing. The scale of the image will ultimately determine the performance of certain metrics within the shape distribution stage. More on the scale of the input images will be explained in the analysis section of this paper.

The computational pipeline (Figure 1-2) consists of processing all input images through the segmentation and shape distribution extraction stages before performing the final classification analysis on an unknown case. This whole pipeline is modular and can be done piecewise. Each image can be described as its own pipeline; allowing multiple images to be computed in parallel, if the computing environment allows for this.

The segmentation process is essentially any process that takes a raw image and converts it into a binary image. The raw image could be binary to start out with, or could use as many bits as necessary to describe the subject, as long as the segmentation process knows how to handle it. The main goal of the segmentation process is to reduce any input into two partitions per image: the regions of interest and the background [57].

The shape distribution extraction process, which will be discussed in more detail later on, involves multiple geometric metrics that will generate a set of shape distributions that can describe each image, which capture geometric features in the image. The shape distribution extraction stage depends on specified regions of interest within a segmented image. Each metric within the extraction stage will generate its own histogram that can be used later for analysis. Most metrics within the shape distribution extraction stage can be computed independently of one another, allowing for parallel computation.

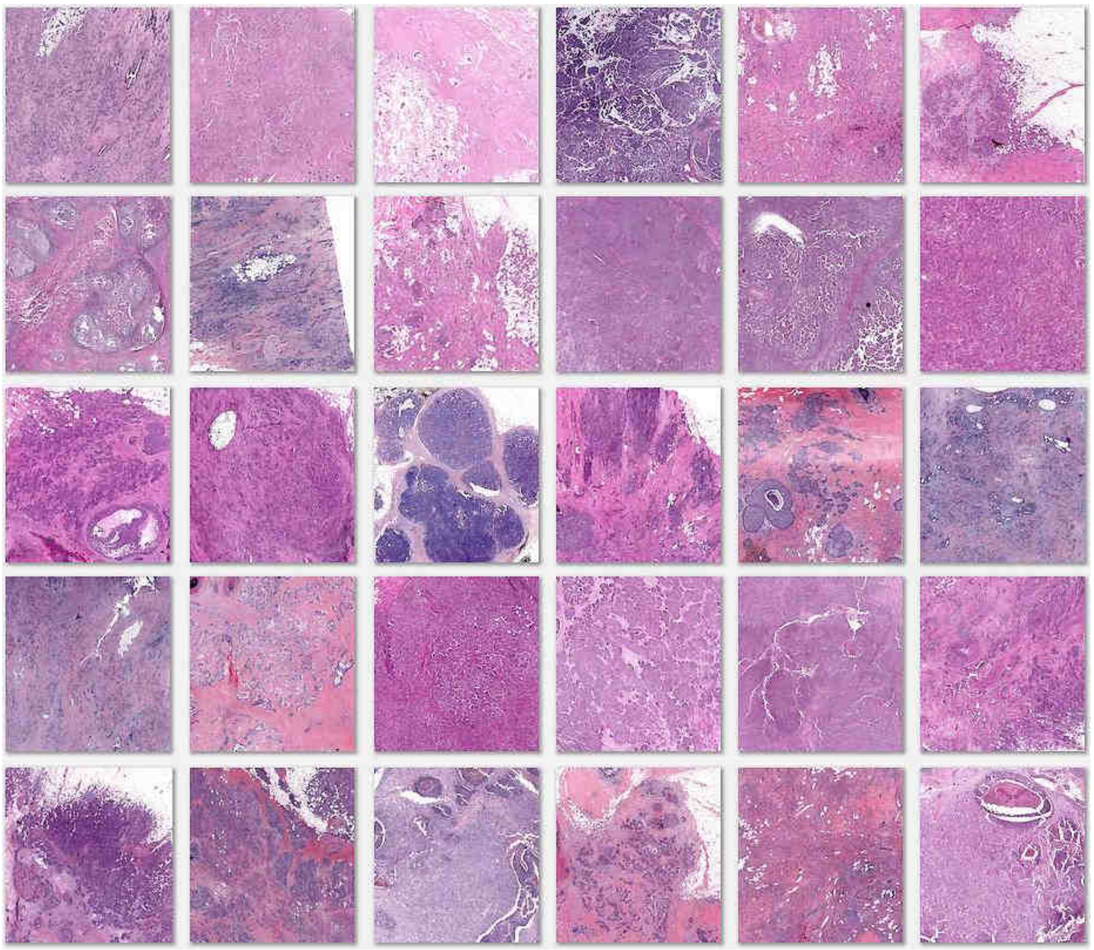

Figure 2-1. Input images

The final stage of the pipeline is the analysis process that will take all histograms (from both the learning and unknown set) and predicts the classification of the unknown case. By this point in the pipeline the entirety of the learning set and the unknown set are all represented in the form of shape distributions. The shape distributions will then be put into the system for determination of its quality in aiding the classification process. The shape distributions, themselves, may also not be fully qualified to classify either. So for example, a shape distribution could have only a certain percentage of itself used for classification and the rest will be discarded. The goal of this stage is to use the given shape distributions and generate the best possible prediction.

2.1 Segmentation

The segmentation process is not the focus of this paper but to fully treat this topic the segmentation process that was used will be described briefly. The segmentation for this thesis has been provided to us by Sokol Petushi and the Advanced Pathology Imaging Laboratory (Drexel University School of Medicine).

The segmentation technique that was used to generate the data for this paper was done using a semi-unsupervised technique. It is used to extract all nucleuar structures within a section of a biopsy. The images that were given to us were from breast cancer patients ranging from histological grade of one to three with no healthy specimens (Figure 2-1). All images were stained using the Hematoxylin and Eosion (H&E) process. The images were all scanned in at a magnification of 10x at a pixel resolution of 6,000 pixels^2 per slide block. We then choose only one slide block out of the numerous images acquired per slide for the segmentation process. We choose the slide block based on what our pathologist deems to be the greatest region of interest within the slide. Our reasoning is that no pathologist will look at everything in a whole slide but only areas of interest within a slide.

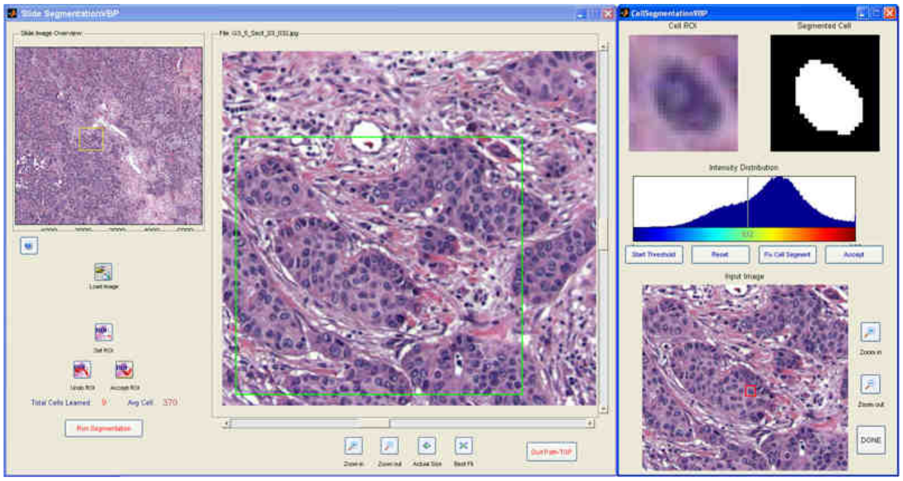

Figure 2-2. Segmentation screenshot

The segmentation process, using a graphical user interface, allows the user to "train" the system into automatically segmenting an image (Figure 2-2). The user is prompted to specify what is defined as a cell. The user will then be shown a segmentation result of what the default settings would give them for the area that they have defined as a cell. The user, at that point, will be able to define, visually, what threshold values they want for the specified cell. This process is refined iteratively as the user defines more cells and manually adjusts the threshold to fit their needs.

After the user has defined up to ten or so cells they can signify the threshold to be accurate for the whole image and run the segmentation on the entire image. The image is then saved as a binary lossless image (Figure 2-3) that can be passed on to the next stage of the pipeline.

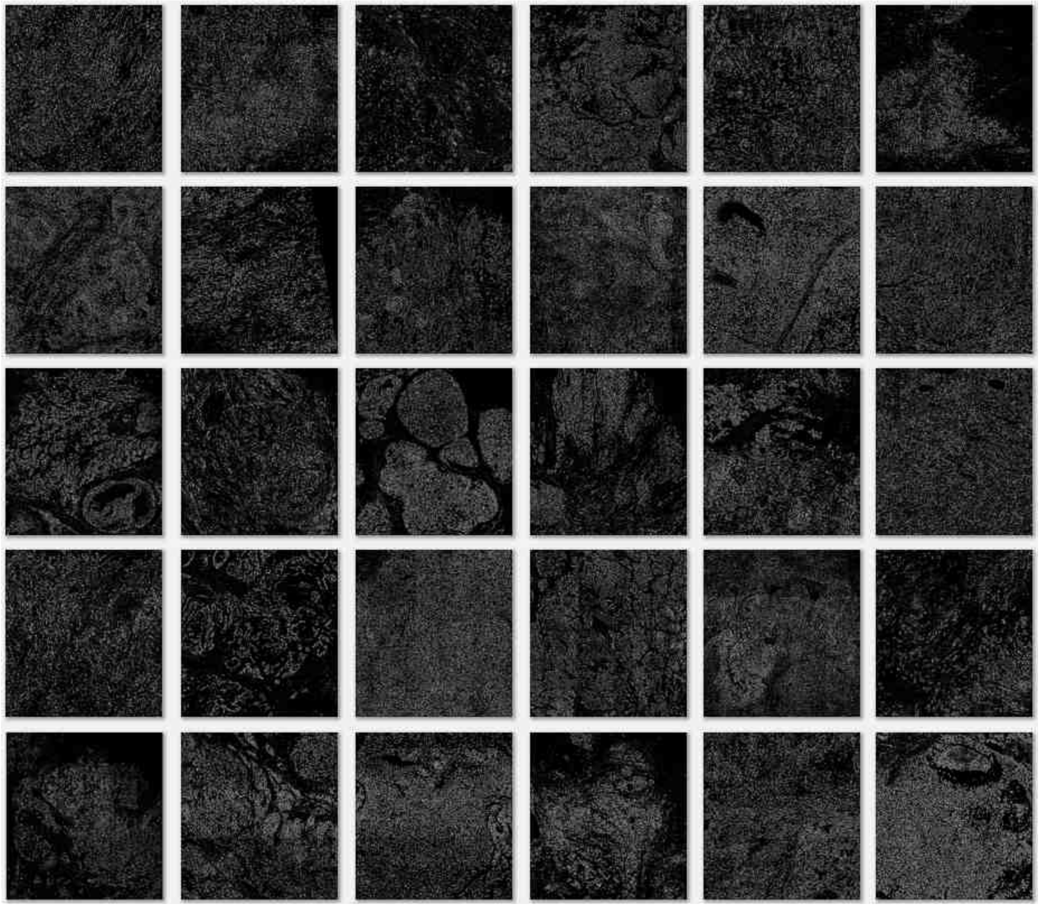

Figure 2-3. Output segmentations

2.2 Shape distribution extractions

The shape distribution extraction process assumes all input images to be in binary format and will always produce a one dimensional shape distribution, represented as a histogram, as its output. Most of the shape functions' computations runs independently of each other and can be computed in parallel given the appropriate computational environment. Some metrics may depend on others or could use the results of other metrics to optimize its own computations. Some of these decisions are made due to computational constraints.

The shape distributions produced by applying the shape functions can be viewed as probability density functions associated with the given image when analyzed with a certain shape function. Each bucket, or a location in the one dimensional histogram, represents the number of occurrences (or probability) of a measurement while using that shape function. For instance, if we are trying to determine how many people are age 25 in a group of people, we would bin everyone with the age of 25 to the bucket of 25. The values in each bucket represent the count of the occurrences of that value within the image when applying the metric. So taking our example of people of age 25, our histogram would have a value of five at the location of 25 if there are five people who are 25 years old. Taking the example further, we would have one histogram for every demographic group that we are working with. Each histogram will be the distribution of age in that particular group.

The metrics that we have defined and implemented for generating shape distributions are inside radial contact, line sweep, area, perimeter, area vs. perimeter, curvature, aspect ratio and eigenvector. The remainder of this section describes how these shape functions have been implemented to generate shape distributions that capture geometric features in histology segmentations.

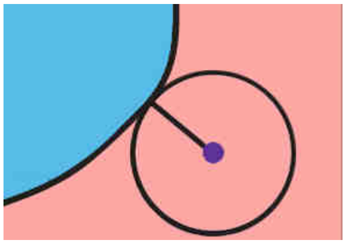

Figure 2-4. Concept of inside radial contact

2.2.1 Inside radial contact

Inside radial contact is a metric that has been used in previous works in geometric matching [29] [18] [47]. The idea behind inside radial contact is to gain insight into the size distribution of an image by probing it with disks. We treat each inside pixel as the center of a disk that is used to probe the shape. The algorithm will determine the maximum radius of a disk that can be fit inside the shape from that pixel (Figure 2-4).

This algorithm can be implemented in multiple ways but it is most efficiently calculated using a distance field transformation of the image [49] [4]. One of the efficiency comes from preserving some information about the image that can be used later for other metrics, for example the curvature metric.

Methods for obtaining a distance field include passing the image through a convolution [30] [24], solving it as a Hamilton-Jacobi equation [5], processing it with a fast marching method [31], or applying the Danielsson distance transform [13] [28]. These approaches are good if the image size is not excessively large. In the case of our dataset, the size can get prohibitively large for this approach. Most of our problems originate back to trying to transform an image more than 10,000 pixels^2.

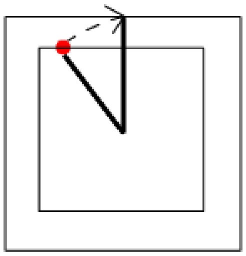

Figure 2-5. Potential error in distance
transform using square flood fill

Because of our hardware issues we had to step back and approached this problem in a temporally less efficient but spatially more efficient manner. Our approach was to take each pixel and do a square flooding on the area, which could detect changes in the pixel color (Figure 2-6). After it found the first pixel of changed color it will then keep expanding past the current location, compensating for the increased distance that may occur along the diagonal (Figure 2-5).

```
for p: all pixels in image
  while distanceList is empty OR there is a distance in
         distanceList that is greater than radius
    for x_val: (p.x–radius) → (p.x+radius)
      if pixel[x_val, p.y+radius] = color_change OR
         pixel[x_val, p.y-radius] = color_change
         add( distanceList, sqrt( (p.x-x_val)2 + radius2 ));

    for y_val: (p.y-radius) → (p.y+radius)
     if pixel[p.x+radius, y_val] = color_change OR
        pixel[p.x-radius, y_val] = color_change
```

```
        add( distanceList, sqrt( (p.y-y_val)^2 + radius^2 ));
    add (finalDistances, max( distanceList ));
```

Figure 2-6. Implementation of square flooding in inside radial contact

Applying the distance transform generates a distance field for the image. The distance field is then transformed into a shape distribution by rounding from all values into the nearest bucket within the representative histogram. Each bucket in the shape distribution represents the minimum distance from a point inside each blob to the contour of the blob.

2.2.2 Line sweep

The idea behind line sweep is similar to that of the inside radial contact in that we are trying to probe the shape of an object with another geometric shape. The way we propose to do this is to pass a line through the whole image and see how many regions of interest it intersects (Figure 2-7). This is inspired by previous work done in [47]. The shape function measures the length of each segment of intersection between the line drawn and the region of interest that it intersects. Each bucket in the shape distribution is a count of how many lines drawn has a segment of intersection that has the length specified by the bucket.

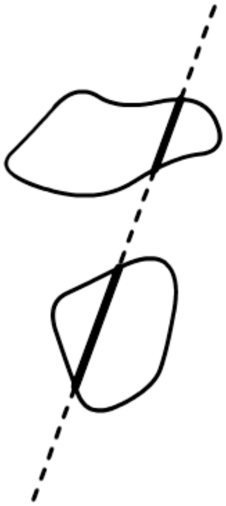

Figure 2-7. Conceptual definition of line sweep

Computationally, the metric will calculate lines from every boundary pixel of the image to all other boundary pixels, ensuring that the start and end pixels are not the same boundary (Figure 2-8). This guarantees that all possible lines that can be processed are processed since the problem is symmetrical, a line going in the direction of point A to point B will produce the same result as that going from point B to point A.

```
boundary = all pixels at the edge of the image
for i: 0 → size(boundary)
 for j: i+1 → size(boundary)
   if ( NOT isOnSameSideAs( boundary[i], boundary[j] ) )
     shootLine( boundary[i], boundary[j] )
```

Figure 2-8. Implementation of visiting boundary pixel for line sweep

The actual line processing algorithm can be any line drawing algorithm that the implementer chooses. The line drawing algorithm we chose to use is the Bresenham line raster algorithm [6]. We chose it because it is fast and the most commonly used line raster algorithm. The only difference with our approach is that instead of drawing a pixel at every raster we do a look at function that determines if there is a transition of colors (Figure 2-9). This keeps track of the starting and ending locations of a line segment that is drawn contiguously through a region of interest. We compute the Euclidean distance between the start and end locations.

```
LOOKAT x, y, I
  if I[x,y] = inside
    if NOT isInside
      isInside = TRUE
      p1 = Point[x,y]

  if I[x,y] == outside
    if isInside
      incrementBucket( lengthList, distance(p1, Point[x,y]) )
      isInside = FALSE
```

Figure 2-9. Implementation of look at in line sweep

Another special concern is usage of image libraries. From many experiments we have discovered that an image library that involve built in virtual swapping should be avoided (in our case, the Image Magick API). Using this library causes problems because this algorithm will sweep the whole entire image every iteration. So if the library swaps in only a portion of the image at any given instance, anticipating localized computation, it will have to clean out the whole image cache in memory repeatedly every iteration. This will produce excessive over utilization of the processor and memory bus for needless operations. This, however, requires the system to have enough memory to store the whole image at once as well as control over the caching of the image library API. If the system memory can't hold the full image then it is highly advised that the developer implement their own caching scheme that will minimize on demand paging within each iteration. Another concern with image libraries is that it is a good idea to avoid any that use class hierarchies and other object oriented overhead, such as the Image Magick API [9] [12] [25]. The computation is already extensive, taking a minimum of eight hours on a 60,000 pixel^2 image; adding object oriented overhead would drastically increase runtime.

The final computation concern of the line sweep algorithm is parallel computation. After some experiments we have discovered that threading the line processing procedure will not improve the computation time at all. After analyzing the system monitor we discovered that when the whole image is in memory with a singly threaded build, CPU utilization is always near maximum with almost no wait time for I/O access. But when we employ a multi-threaded build that utilizes symmetric multithreading (better known as Hyper-threading in the Intel core) the CPU utilization of both cores dropped below 60%. From this we can infer that the main memory bus is only able to provide enough throughput for a single core computation. Anything more would cause I/O wait time for the process.

2.2.3 Area

The area metric is computationally the simplest of all metrics. It finds the area, in pixels, of all regions of interest (defined by inside regions) within the image (Figure 2-11). Applying the area metric produces a profile of the size distribution of regions of interest in the given image. The difference between area and inside radial contact is that inside radial contact finds a size distribution on the pixel level whereas the area metric finds a size distribution on the regions of interest level. The shape distribution generated by area produces a histogram that measures the area of a complete blob. Each bucket within the area shape distribution represents the count of blobs of the specified area.

The implementation of the area metric is very simple in that it depends heavily on a recursive procedure. Once it finds an inside pixel it will try to flood the area looking for other inside pixels until it hits an outside pixel. It will do this until no more inside pixels can be explored within the region of interest, in which case it will count the number of pixels inside the region and bin itself into the appropriate bin and move onto an inside pixel of the next region of interest. This implementation uses a residual image to insure that no region of interest is binned twice. This residual image will keep track of all pixels visited by the algorithm already. It needs to be looked at along side the actual image simultaneously. This image can be the same size as that of the original image, if memory allows, or it could be a block of the image. Some form of book keeping is needed to make sure that the residual image matches up with the location of the current read in the original image (Figure 2-10).

```
...
for p: every pixel in the image
  if NOT findArea(p.x, p.y, I, R) = 0
    add (finalArea, findArea(p.x, p.y, I, R));
...

findArea x, y, I, R
  area = 0
  if I[x,y] == inside AND R[x,y] == notRead
    area = area + 1;
    R[x,y] = Read
  else
    return 0

  area = area + findArea (x+1, y, I, R);
  area = area + findArea (x+1, y+1, I, R);
  area = area + findArea (x+1, y-1, I, R);
  area = area + findArea (x, y-1, I, R);

  area = area + findArea (x-1, y, I, R);
  area = area + findArea (x-1, y+1, I, R);
  area = area + findArea (x-1, y-1, I, R);
  area = area + findArea (x, y+1, I, R);

  return area
```

Figure 2-10. Implementation of area

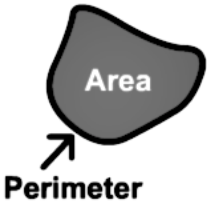

Figure 2-11. Concept of area and perimeter

2.2.4 Perimeter

The perimeter metric is similar to the area metric in that it also deals with individual regions of interest instead of pixel by pixel statistics. This metric counts all interface pixels in a region of interest (ROI) (Figure 2-11). An interface pixel is a pixel that is in a ROI and where there is a change from inside to outside at a neighboring pixel. The reason for this metric is to measure the distribution of surface areas of the regions of interest, since this is a cross section of a three dimensional object. Biologically this is important in that it measures how much nutrients a region can get. The more surface something has the more nutrients it will get.

There are several choices of implementation for this metric. Some of them could be detecting all edges after passing the image through edge detection using such things as the Laplace filter and its equivalent [26] [27]. But due to the fact that we have already find all the ROI from the area metric we can apply that information to make this metric more efficient. Starting with each ROI we can check all of its pixels with an interface test that checks for the crossover from inside to outside (Figure 2-12). Each pixel that gets picked up gets added to the perimeter size count for that region of interest, which is then binned to the final histogram.

```
...
for b: all blobs in image
  pixelCount = 0;
  for p: all pixels in b
     if isInterface(p.x, p.y, I)
```

```
        pixelCount = pixelCount + 1;
    add( finalPerimeter, pixelCount );
    ...

  isInterface x, y, I
    if I[x,y] == outside
      return FALSE

    if NOT I[x-1,y] == I[x,y]
      return TRUE
    else if NOT I[x,y-1] == I[x,y]
      return TRUE
    else if NOT I[x+1,y] == I[x,y]
      return TRUE
    else if NOT I[x,y+1] == I[x,y]
      return TRUE
    else if NOT I[x+1,y+1] == I[x,y]
      return TRUE
    else if NOT I[x-1,y-1] == I[x,y]
      return TRUE
    else if NOT I[x-1,y+1] == I[x,y]
      return TRUE
    else if NOT I[x+1,y-1] == I[x,y]
      return TRUE
    else
      return FALSE
```

Figure 2-12. Implementation of interface detection in perimeter

2.2.5 Area vs. Perimeter

Area vs. perimeter is a metric that combines the previous two metrics into one metric. The reasoning behind this metric is to try to determine the surface to volume ratio of a region of interest. This is one of the major metrics in determining the aggressiveness of a biological object. The more surface area a cell has per volume of mass the more aggressive it can grow. This happens because more surface area is in contact with its surroundings, further advancing its nutritional acquisition.

The implementation of this metric is fairly straight forward. The ratio is the area divide by the perimeter for each ROI and the ratio is then binned. A post process must be applied to the value but that will be discussed later in this paper.

2.2.5 Curvature

The curvature metric is very similar to the area vs. perimeter metric in that it is trying to determine the relative relationship between the surface area and the volume of a region of interest, since the rougher a surface is the more surface area it must have to produce the roughness. The difference between this metric and area vs. perimeter is that this is a distribution of roughness along individual perimeter pixels. This can give us a different measurement of the ratio between surface and volume since it is a whole magnitude smaller in scope than area vs. perimeter.

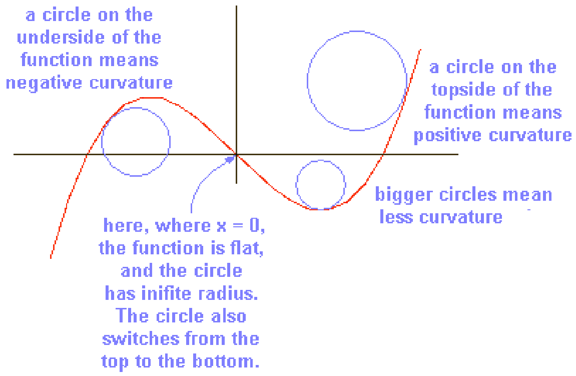

Figure 2-13. Conceptual definition of curvature

Curvature can be defined by the smallest circle that can fit a given local area of a curve at a specific interval (Figure 2-13) [10]. Curvature is 1 / (radius of the circle). What this essentially comes down to is that the larger the approximation circle's radius is the smoother the curve is at a given point, and the lower the curvature. What we found is that if we take the distance field generated from the inside radial contact metric we can easily apply a methodology from volume graphics to solve this problem. We have thus proposed to use the level set curvature formulation [31] to solve our problem (Equation 2-1) on a blurred image of the binary segmentation.

$$\nabla \cdot \frac{\nabla \phi}{\left|\nabla \phi\right|} = \frac{\phi_{xx}\phi_y^2 - 2\phi_x\phi_y\phi_{xy} + \phi_{yy}\phi_x^2}{\left(\phi_x^2 + \phi_y^2\right)^{3/2}}$$

Equation 2-1 Level set curvature

The implementation of this formulation is straight forward on a blurred gray scale image produced with a convolution. The binary image is passed through a Gaussian kernel one ROI at a time, so as to never duplicate more than one percent of the image during any one calculation. The kernel width was two pixels with a sigma of three. Once we obtained a Gaussian blurring of the binary image for a specific ROI, we calculate Equation 2-1 at the perimeter pixels using the intensity values of the blurred copy (Figure 2-14).

```
...
for p: all pixels in the image
  if isInterface(p.x, p.y, I)
    add(finalCurvature,abs(signedCurvature(p.x, p.y, I));
...

signedCurvature x, y, I
  dx = (I[x+1,y] – I[x-1,y]) / 2.0
  dy = (I[x,y+1] – I[x,y-1]) / 2.0

  dxx = ((I[x+2,y]-I[x,y])/2.0 – (I[x,y]-I[x-2,y]/2.0) / 2.0
  dyy = ((I[x,y+2]-I[x,y])/2.0 – (I[x,y]-I[x,y-2]/2.0) / 2.0

  dxy = ((I[x+1,y+1]-I[x-1,y+1])/2.0 - (I[x+1,y-1]-I[x-1,y-
         1])/2.0) / 2.0

  return (dxx*dy*dy - 2*dx*dy*dxy +dyy*dx*dx)/ pow(dx*dx +
          dy*dy, 3.0/2.0)
```

Figure 2-14. Implementation of curvature

All curvature values from perimeter pixels are binned without sign. The sign of the curvature is irrelevant for our computation since we are only concerned about the absolute curvature of a pixel.

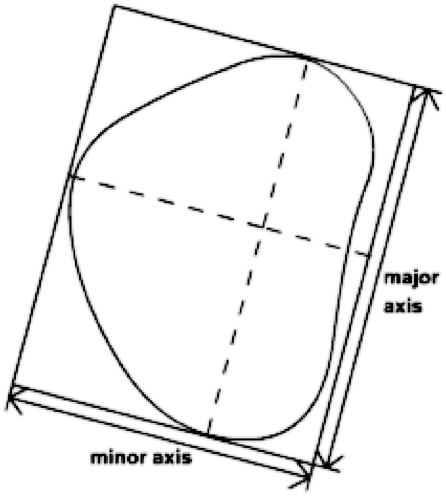

Figure 2-15. Conceptual definition of aspect ratio

2.2.7 Aspect Ratio

Aspect ratio is a metric that evaluates the overall shape and dimensions of an object. It divides the object's shortest span by its longest span. The concept can be visualized by tightly fitting of a rectangle around an object and dividing the shortest edge by the longest edge (Figure 2-15). This measure is applied to all regions of interest individually.

Aspect ratio is one of the two metrics that depends on eigen systems. Aspect ratio is the ratio between the length of the major and minor axis of an object. It is inherently independent of directions, as it builds its own reference coordinate system. The mathematical reason behind using such a system is that each region of interest may align itself in a different direction to the image but for every one of them we still want to extract an aspect ratio that is true to the region. The eigen system takes in all data points, in our case all pixels from the region of interest, and defines both the eigenvalues and eigenvectors (Figure 2-16) [55]. The eigenvectors are the normalized vectors that define the local reference coordinate (to be discussed more in the next metric) and the eigenvalues describe how far the dataset stretches along the eigenvectors.

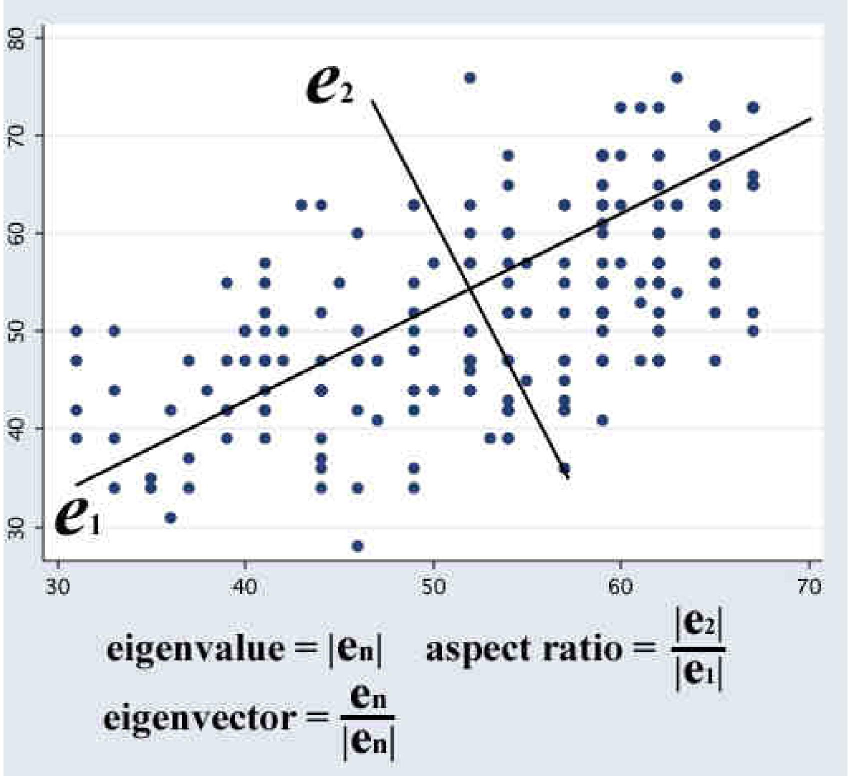

Figure 2-16. Definition of eigen systems

In building the eigen system we must first build a covariance matrix before we can extract the eigenvalues and eigenvectors [8]. The covariance matrix is a matrix that defines the variance within a set of random elements [15]. In our case our random elements are the pixels in each region of interest. The variance within our system is the distance between each pixel and the centroid, center of mass, in a ROI. The covariance matrix that we can construct will be the overall covariance of a ROI (Equation 2-2).

$$\begin{bmatrix} x^2 & xy \\ xy & y^2 \end{bmatrix}$$

Equation 2-2 Definition of covariant matrix
in terms of a ROI's pixels' x and y
coordinate

After the covariance matrix is generated the eigenvalues and eigenvectors must be extracted from it. The technique used is the real symmetric QR algorithm described by Golub and van Loan [21]. The eigenvalues and eigenvectors are then sorted by eigenvalues to distinguish between the major and minor axis. The final computation is produced by dividing the eigenvalue of the minor axis (the one with the smaller value) by the eigenvalue of the major axis (the one with the greater value). We divide the minor axis by the major axis (as opposed to major by minor) to produce consistent results in the range of 0.0 and 1.0 for the final value. The final aspect ratios for each ROI are then binned.

2.2.8 Eigenvector

The eigenvector metric is related to the aspect ratio metric in that it may make use of the other half of the eigen decomposition (Figure 2-16). This metric measures the distribution of shape alignments within an image. It takes each ROI and measures the angle between (cosine of the angle to be exact) the ROI's direction and the average direction of all regions within an image. The biological reason behind this is that this analysis is what many pathologists use behind the scenes. From my interview with John Tomaszewski (a pathologist at the University of Pennsylvania) I discovered that the Gleason indexing system for prostate cancer is almost completely based off of the measurement of structural entropy within a given section. The more randomness exists within a section the higher the grade. He also claimed that this measure helps distinguish between cases in many other specimens as well. So inspired by this concept we have devised a metric that attempts to capture this aspect of histology.

The implementation of this metric first determines the average the major axis of all the ROI in an image. The major axis of the ROI is the eigenvector associated with the greatest eigenvalue of the ROI. After obtaining the average major axis of all the ROI it then calculates the dot product of all the ROI major axes with the average major axis. The dot product is the representation of the cosine of the angle between the average major axis and the major axis of each region to be binned [55]. The resulting dot product is then binned into the histogram after having 1.0 added to it (to keep the values positive since it ranges from -1.0 to 1.0).

2.3 Computational Performance

For a full treatment of how well our pipeline performs we will first state the computational environment that we are working with:

- CPU: AMD Athlon 64 X2 4400+ (Dual core, 2.2 GHz, 64-bit)
- Memory: 3 GB, DDRAM, PC3200 (400 MHz)
- Hard drive: 475 GB, Hardware RAID 5, SATA I over PCI interface
- Operating System: Fedora Core 6 x86_64 build, 20 GB swap space
- Compiler: GCC 4.1.2 x86_64 build
- Image library: Image Magick (Magick++) 6.2.8 x86_64 build

The following are the average runtime of all our metrics when given an image of 60,000 pixels^2:

Table 2-1 Performance of all metrics

Metrics	**Runtime**
Inside radial contact	7 min
Line sweep	8.5 hours
Area	3 min
Perimeter	3 min
Area vs. Perimeter	3 min
Curvature	20 min
Aspect Ratio	2.5 min
Eigenvector	3 min

It should be noted that, computationally, the distance transform is the bottleneck of both inside radial contact and the curvature metric. The time taken by the curvature metric is much greater than that of the inside radial contact due to the "lazy" approach taken by the inside radial contact. The inside radial contact metric only completed a distance transform for the inside pixels only, whereas curvature has to do both. Aspect ratio and eigenvector metrics are both bottlenecked on the eigen decomposition of the covariant matrix. Line sweep takes the time indicated to run on our system primarily due to the number of cache misses that force the system to over-utilize the north-bridge of the system bus.

2.4 Distribution analysis

After the shape distributions were generated they were processed by a variety of analysis to determine the usability of the measures as well as the overall performance of our pipeline. The analysis process involved both manual and automatic schemes as we considered all outcomes.

The first step involved was post-processing the histograms to insure that the data are not sparse or noisy. This will be described in more detail in section 3.2. After the post processing we viewed all the histograms in the form of a graph. The graphs were laid out in a form that has the bins on the X axis and the counts in each bin as the Y axis. Each histogram starts at the first non-zero bin. We also looked at the graphs of all cases laid out together to determine if any trends were evident. Overall we found some metrics appeared to be suitable and others were not as.

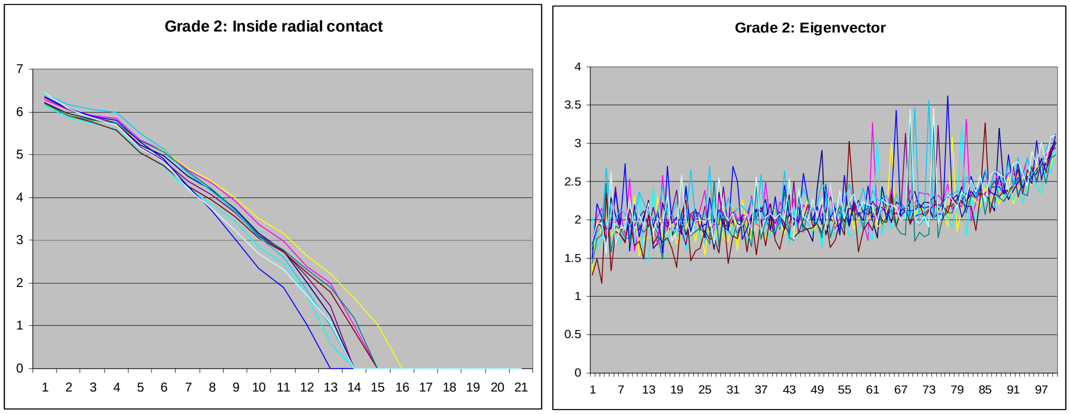

Figure 2-17 Histogram of inside radial contact and eigenvector

For example, we present the shape distributions for inside radial contact and eigenvector metrics in Figure 2-17 in all Grade 2 samples. For histological grade prediction, it is clear that there is some consistency between the inside radial contact distributions, whereas there is a great deal of variability within eigenvector distributions with a high amount of local oscillation.

In later chapters we apply K-nearest-neighbor classification to the shape distributions using the Earth Mover's Distance as our edit distance, which is explained later in Chapter 4. We then take the classifications produced by the K-nearest-neighbor algorithm and examine the results using the cluster analysis metrics of precision, recall and F-measure.

Chapter 3

DATA PROCESSING

The data entering the computational pipeline begin as binary segmentations of the histological slide images and are then transformed into shape distributions, represented as histograms, that capture the structure of the entire image in a series of numbers that can be viewed as a signature of the image. These histograms are a description of how often a certain value occurs when a certain geometric metric is applied to the image. Based on how certain metrics perform, not all pixels in the binary segmentations are desirable as well as not all numbers generated by each measure are needed for or relevant to the final decision making process. Besides the undesirable results of the immediate input there may also be undesirable results that are attributed to processing much earlier in the whole process. This chapter will address and talk about all these concerns of the computational pipeline.

3.1 Preprocessing

During the segmentation process there is a possibility of capturing some regions that are truly regions of interest. This may happen for a variety of reasons due to the fact that segmentation is an optimization process. Utilizing the traditional segmentation metric, the Mumford-Shah framework [39] for measuring the performance of a specific segmentation, there are three functionals that measure the degree of match between an image, $g(x,y)$, and its segmentation, $f(x,y)$ (Equation 3-1).

$$E(f,\Gamma)=\iint_{R-\Gamma}\|\nabla f\|dxdy+\mu^2\iint_R(f-g)^2dxdy+\nu|\Gamma|$$

Equation 3-1 Mumford-Shah framework

In the three functionals in Equation 3-1, we observe that the first functional represents the energy still remaining in the image, the second functional represents the difference between the original image and the segmentation and the last functional represents the length of the boundaries of each region (Γ). Within this formulation there are two constants that a segmentation can modify to tailor its specific needs, μ and ν. The constant μ specifies the amount of error that the final segmentation can have from the original image and the constant ν specifies how smooth the boundaries can be.

So given the classic segmentation analysis we can see that the two constants specifying the correctness of a segmentation are purely based on two factors of the segmentation, how big (which also implies how many) and how smooth are each regions of interest within the segmentation. This adds a complication since every image has its own unique segmentation. As we have discussed earlier in our computational framework, we depend on the accuracy and precision of those two properties for each region of interest.

Table 3-1 Data preprocess

	Inside radial contact	Line sweep	Area	Perimeter	Area vs. Perimeter	Curvature	Aspect Ratio	Eigenvector
Examine inside pixels only	X		X	X	X	X	X	X
Consider only when 64<Area<1500	X	X	X	X	X	X	X	X
Consider only when 1:6<Aspect Ratio	X	X	X	X	X	X	X	X
Examine perimeter pixels only				X	X	X		

To keep qualities consistent in our images for the analysis stage, we have applied the filtering of information presented in Table 3-1. This filtering will narrow the range for each image down to appropriate values for each individual metric. For most metrics it was not necessary to look at outside pixels except for line sweep. The line sweep metric needs to process all pixels during its sweeping process.

The reasoning behind the area filter is to make sure that we are not introducing noise or segmentation errors in the shape analysis. We observed our segmentations closely and discovered that regions of interest smaller than 64 pixels in area are too small to be of a nuclear structure, but instead are products of over segmentation. The regions of interest that are larger than 1500 pixels in area tend to be several nuclear structures clumped together, an artifact of under segmentation. Another cause of large regions of interest within the segmentation can be caused by tubular formations (Figure 3-1) or other non-nuclear structures within the tumor. Those are not what we wish to analyze in this study and to fall into structures larger than 1500 pixels in area. By filtering out those two size categories of regions of interest, we were able to maintain some form of quality control over what is passed into the shape distribution process.

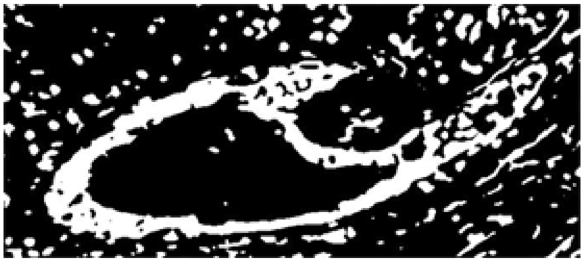

Figure 3-1 Segmentation error with large
tubular formations

The aspect ratio filter was used to filter out anything that is too "skinny" and may resemble more noise. This may at first seem like a good way to get rid of strands of dust particles or other form of pollutants that may get onto the slide during the scanning process... and it may very well do that if the slides were not scanned in cleanly... but more importantly it is used to further filter errors from the segmentation. This could potentially help filter out background noise that many biological images may have. If for example you have many cells lined up like a wall along some membrane and you were trying to segment the image. If the background is a similar color to the nucleus structure, the segmentation process would not necessarily pick that up as a region of interest. This filter would essentially eliminate those "mistakes" from the segmentation.

The perimeter filter is for optimization purposes. It is used so that all metrics that perform a computation at a perimeter pixel do not waste computation on unnecessary pixels. The only two metrics this would affect is the area vs. perimeter and the curvature metric.

Table 3-2 Histogram binning multipliers

	Multiplier
Inside radial contact	1x
Line sweep	1x
Area	0.10x
Perimeter	1x
Area vs. Perimeter	10x
Curvature	50x
Aspect Ratio	100x
Eigenvector	50x

3.2 Post process

After we have generated all the shape distributions from the filtered segmentations we observed that some of the results of applying the metrics didn't fall naturally into a significant number of integer bins. To increase precision we then multiplied all metric results, to increase the number of bins needed to represent the data. We decided that a reasonable bin count was between 100 and 350, with the exception of inside radial contact (which had a count of up to 21). This was done so that details would not be lost and to ensure that all shape distributions had approximately the same bin count. This is especially important in metrics where we always divide a smaller number by a larger one, e.g. aspect ratio. The range of outputs for those will always be from 0.0 to 1.0. It must be multiplied by a larger number to keep everything from binning to 0. So to deal with that problem we have applied multipliers to the results produced by applying the metrics in order to properly scale the range of the metrics' output (Table 3-2).

Table 3-3 The before and after of the data range after post processing

	Before	**After**
Inside radial contact	1-22	1-22
Line sweep	1-141	1-141
Area	64-1500	6-150
Perimeter	28-450	0-350
Area vs. Perimeter	0.12-1.02	12-102
Curvature	0-21	0-349
Aspect Ratio	0.1667-1.0	17-100
Eigenvector	0.0-2.0	0-100

The multipliers for inside radial contact, line sweep and perimeter were kept at one because their bin counts were acceptable. The original range for the area metric went up to over one thousand, which was too large for our system to handle computationally using the Earth Mover's Distance (details in chapter 4), and had to be scaled down to allow for a more manageable size. Everything else had to be expanded due to their extremely small original range. After the expansion, we had to do a preliminary cutoff in the higher ranges for curvature and perimeter due to the obvious sparseness of the data after a certain value where there are large gaps between values that lead to only small bucket sizes. Aspect ratio had to be scaled by 100 due to the fact that it originally ranges from 0.0 to 1.0. Eigenvector had to be scaled by fifty due to the fact that it ranges from 0.0 to 2.0 from the linear shift of 1.0. Aspect ratio originally ranges from 0.0 to 1.0 because at best, it can be square, where the ratio is 1:1 and the worst is actually only 1:6 due to filtering imposed during the preprocessing. The eigenvector metric always produces results from -1.0 to 1.0 before the linear shift due to the nature of the metric definition. Because of the way that it is set up the

Table 3-4 The before and after of the bucket count after post processing

	Before	**After**
Inside radial contact	21	21
Line sweep	140	140
Area	1436	144
Perimeter	422	350
Area vs. Perimeter	1	90
Curvature	21	349
Aspect Ratio	1	83
Eigenvector	2	100

eigenvectors can only range between 0 and 180 degrees from the average direction. The reason is that if it is more than 180 degrees or less than 0 degrees of the major axis it would become redundant since the definition of an eigen system defines that the eigenvectors that forms it is the orthonormal basis of the vector space [55]. The value of cosine(0) in degrees is 1.0 and cosine(180) in degrees is -1.0. The ranges of values produced by each metric before and after scaling are presented in Table 3-4. The bucket counts produced by each metric before and after scaling are presented in Table 3-4.

We discovered that logarithmic scale is better than a linear one to one mapping of the values within each bucket. One of the initial reasons for doing this is that everything in natures seems to be either in an exponential scale or logarithmic scale. Take for example sound decay (exponential) and population growth (exponential). We also discovered that a variety of image analysis texts also suggests a logarithmic scale over linear one to one scale [11] [58] [22] [17]. After observing our data, we did see an exponential growth in value in most cases.

The other question we considered was do we need analyze all bins in each histogram? The histograms are very good in that they describe the structures in the entire image completely according to one metric, but are all the information contained in them significant? Depending on the shape distribution we are working with, we argue that some of its bins may be discarded. In certain cases we argue that using all bins will add significant noise/randomness into the analysis, and this makes the analysis meaningless. So to increase the significance of and to minimize noise, and therefore improve the predictability of the data, we propose to crop the shape distributions to those portions with less noise/randomness and deemed significant.

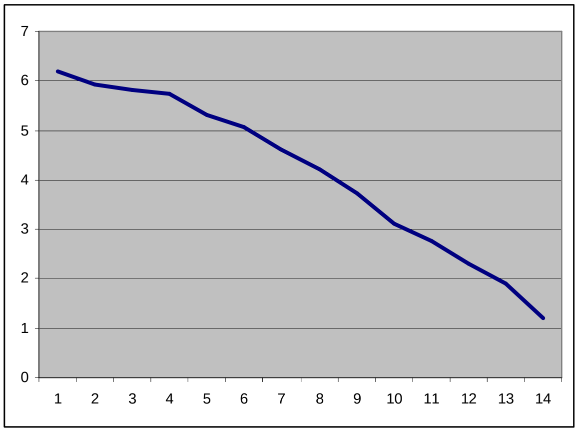

Figure 3-2 Example of inside radial contact's histogram

A shape distribution generated by a metric that produces mostly "valid", i.e. data with minimal noise, can be seen in Figure 3-2. The example graph shows the histogram of a typical inside radial contact mapped with a logarithmic scale. Inside radial contact produces an extremely well behaved shape distribution due to its small size (14 bins) and lack of local variation. The bin size of all inside radial contact shape distributions does not exceed 21 buckets, making this an easy shape distribution to work with. But for example, Figure 3-3 contains a shape distribution produced from the curvature metric that has a very sparse and noisy tail that could potentially produce numerical instability during analysis. As we will see later, the Earth Mover's Distance, which is our shape distribution metric for similarity, has less error and performs much faster with smaller shape distributions.

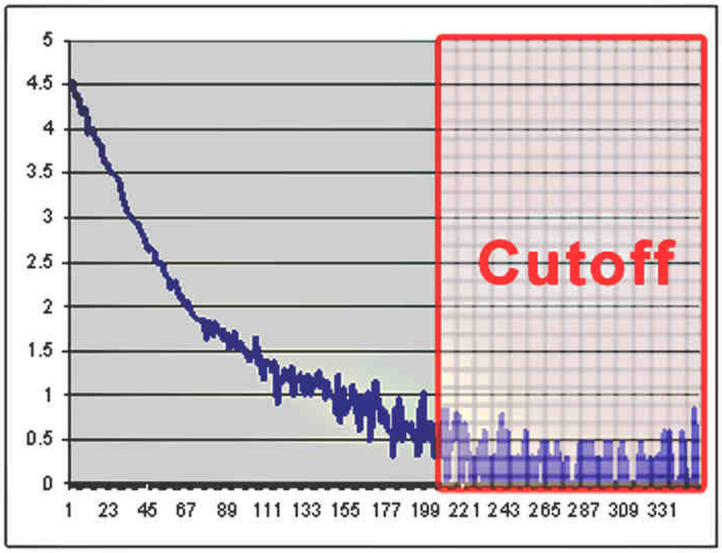

Figure 3-3 Example of curvature's
histogram

The approach taken to remove noisy tails from the shape distributions was to take all the images in each classification group (predefined by pathology, in our case the Nottingham indexing scale) and standardize the bin ranges for all the associated shape distributions. This essentially means that we calculated the absolute bin range for each group and filled each shape distributions' undefined bins with zero count. This will guarantee that every distribution within the same group will all start and end at the same bin location. The maximum bin location for all shape distributions produced by a particular metric is defined to be the maximum of all the first zero bin locations. This effectively removes the "noisy tails" from the shape distributions. If the shape distributions have zero bins preceding any significant portions then the minimum bin will be defined by the minimum zero bin of all the zero bins preceding the data. By doing this we will ensure that all processed shape distributions have noise removed from their fronts and tails. The only problem that this could cause would be an abnormal cutoff for shape distributions with a zero bucket in the middle. Fortunately for our data, this did not occur.

Generating the shape distributions from the breast cancer segmentations and applying our filtering and processing produced the shape distributions ranges as presented in Table 3-5.

Table 3-5 Shape distribution ranges for all metrics

	Total Span	Usable region
Inside radial contact	1-22	1-20
Line sweep	1-141	1-134
Area	7-150	7-145
Perimeter	0-350	0-242
Area vs. Perimeter	12-102	12-91
Curvature	0-349	0-209
Aspect Ratio	17-100	17-92
Eigenvector	0-100	0-100

3.3 Pre-segmentation dependencies

The last issue regarding data that needs to be mentioned are potential problems produced by the pre-segmentation phase of the pipeline. Errors from this phase may have been propagated from the segmentation phase and could have skewed the distributions of our shape distributions and, ultimately, the predictive power of the final stage.

The first problem that we noticed throughout our work was that the level of magnification used during the scanning stage of the pipeline might skew the results of our metrics. We see the ill effects of magnification mostly in the curvature metric where a majority of the shape distributions exhibit sparse, noisy tails. Examining the segmentation in Figure 3-4 it can be seen that very little of the roughness in most structures is captured. In fact only the major turns on the contour of each region is captured. It is clear to see that this kind of segmentation can not differentiate very much between two histological images.

Despite of the error that this causes in the curvature metric, this could be the perfect magnification for other metrics. So we do feel that it might be good idea to consider multiple levels of magnification when analyzing histology segmentations. We need to discover the optimal level of magnification for each metric to increase the predictability of each metric. This is also the procedure used by a pathologist when examining a section. He/she will first view the slide at a low magnification, identify the area of interest and zoom in to the region for further analysis. Each level of magnification can lead the pathologist to a different conclusion about that section.

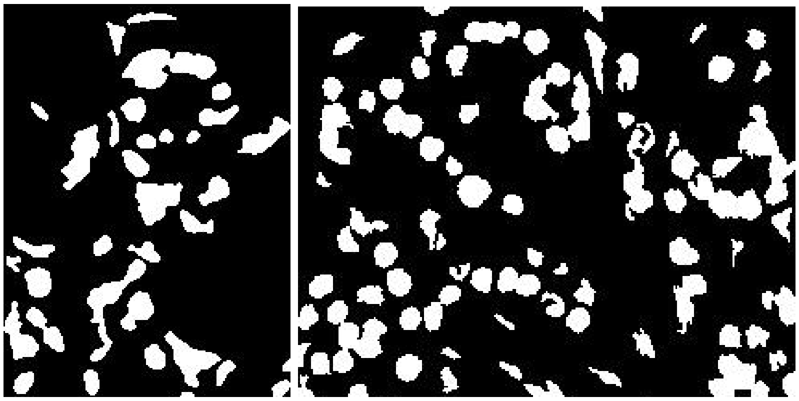

Figure 3-4 Multiple segmentations at 10x magnification

The second and last concern for the pipeline prior to segmentation is the morphological distortion applied to the section when it is stored in a slide. According to the pathologist we work with the shape of cells and different tissues can be distorted when it's cut and compressed between two panes. This distortion could lead to inaccuracies within the aspect ratio and the curvature metric. This, however, should not cause any inaccuracies in the area and perimeter metric.

Chapter 4

ANALYSIS

Once the shape distributions are generated, they are analyze to determine how effectively each metric correlates an image to its histological grade. We have devised a few methods for analyzing the histograms that represent the shape distributions. The key to quantifying the effectiveness of a metric is to determine if it can correctly identify the classification of a sample of a known grade.

In our first approach we attempted to classify clusters of shape distribution in a high dimensional space. We treated every case as a point in a high dimensional space and attempted to find clusters of classification groups using a L-2 norm. This led us to unpromising data that does not seem to cluster well.

The second approach we took was to try to determine the classification of a case based on querying our known cases using K-nearest-neighbor. We attempted to perform such an analysis on the whole histogram that represents the shape distribution and validated it against standard metrics used in information retrieval (precision, recall and F-measure [48]). By performing the validations we discovered that by comparing windows of sub-regions within the histograms instead of the whole histogram we would be able to achieve better performance with each geometric metric.

After performing the validation on all analysis of the sub-regions we were able to determine certain criteria that would potentially gain the best performance with our given data set for each geometric metrics. Due to the size of our data we were able to only make suggestive claims as to how well each of our geometric measures performed in our given scenario. All this and more will be described in this chapter.

4.1 Earth mover's distance

The Earth Mover's Distance (EMD) is an algorithm devised in Stanford in the late 90s for distribution analysis [51]. The purpose of EMD is to compare two histograms and purpose a measure of the similarity between the two using an optimization algorithm. Similarity, defined by EMD, is the minimal energy needed to transform one distribution into another. It can be described using the analogy of trying to fill a set of holes by moving dirt from a mound of dirt. We have chosen EMD over other algorithms primarily due to the success that was attributed to it in the computer vision domain [50].

The reason that we chose to use EMD over all other measures was because it was considered the optimal algorithm for comparing two histograms. One of the primary reasons why EMD is better for our purpose is due to EMD's capability to compare between two histograms of varying lengths. EMD has a nice property of treating all vectors given to it as distributions, where size differences do not cause computational problems as do most histogram based algorithms [51].

After using EMD for awhile we also noticed a few properties of it that are worth noting. One of them relates to the previously stated property that we have observed. When given two distributions of varying length EMD will treat them as if they are the same length starting at the same bin location. What that means is that if you have one histogram starting at *n* and another starting at *n+m*, EMD will treat the histogram as if both started at the same location. That is a problem if we are comparing regions. Due to the displacement and potential scaling, padding in zeros in the front and back of a histogram to normalize the length will cause the EMD to produce a different result when compared to unpadded comparisons.

Another issue with EMD is that due to the arbitrary offset and length it creates for two histograms it will view each bin as a percent of the total mass. The sum of all bin values will sum to one. This is a good property for histograms of small values but will get numerically unstable as the histogram bin count increases. This is also a problem if the total sum of all values is large as well. We have tackled this problem by converting all histograms to log scale. A problem with log scale is that there is also a potential for sparse data to create numerical instability as well. A sparse histogram will cause the algorithm to require a higher EPSILON to converge, which causes potential for more error in the final result.

The last issue with EMD that is worth mentioning is that it is not linearly additive. What that means is if you take histogram H1 and histogram H2 and you do an EMD calculation on it, it will come up with result A. But if you break up H1 and H2 to be four halves instead of two wholes, the sum of EMD(FirstHalf(H1), FirstHalf (H2) + EMD(SecondHalf(H1, SecondHalf (H2)) will not equal EMD(H1, H2). The reason behind this is the fact that EMD is an optimization problem and therefore does not grow linearly. Therefore there is no simple means to breakdown the histograms and compute it by parts. This is important in that the EMD calculation will be directly constrained by the size of the problem. Though this problem shouldn't really be an issue due to the size of most problems, it can nevertheless be handled by either scaling or trimming ends of the histograms if the size of the problem really calls for it.

4.2 Shape distribution sub-regions

The one consideration that needs to be taken into account is sub-regions within each distribution. As discussed in data post processing, we hinted at the fact that maybe the entire histogram would not be needed for prediction and matching. As we proceeded with our experimentations we discovered that we only need certain sub-regions of a histogram to produce acceptable comparison results, even after filtering out the sparse regions (as explained in data post processing).

One of the key ideas behind finding a good sub-region for comparison is to find a region of good separation between classification groups. A visual inspection, as shown in Figure 4-1, shows that it is clear that certain sub-regions are better separated than others. The sub-region does not necessarily have to separate all classification groups in any sub-region but only has to have a good consistent separation between at least two of the classification groups. If any two or more geometric measures, on their own individual sub-regions of best separation, can eliminate two out of three grades that a case can be, we can still predict what grade a case is. Figure 4-1 shows a visual representation of two average histograms that represents shape distributions of two histological grades for each individual geometric measure that we have implemented with the exception of eigenvector, which is ambiguous in respect to separation. As we can see from Figure 4-1, we have at least one geometric measure that has a significant sub-region of good separation for every possible combination of pairing between the three histological grades.

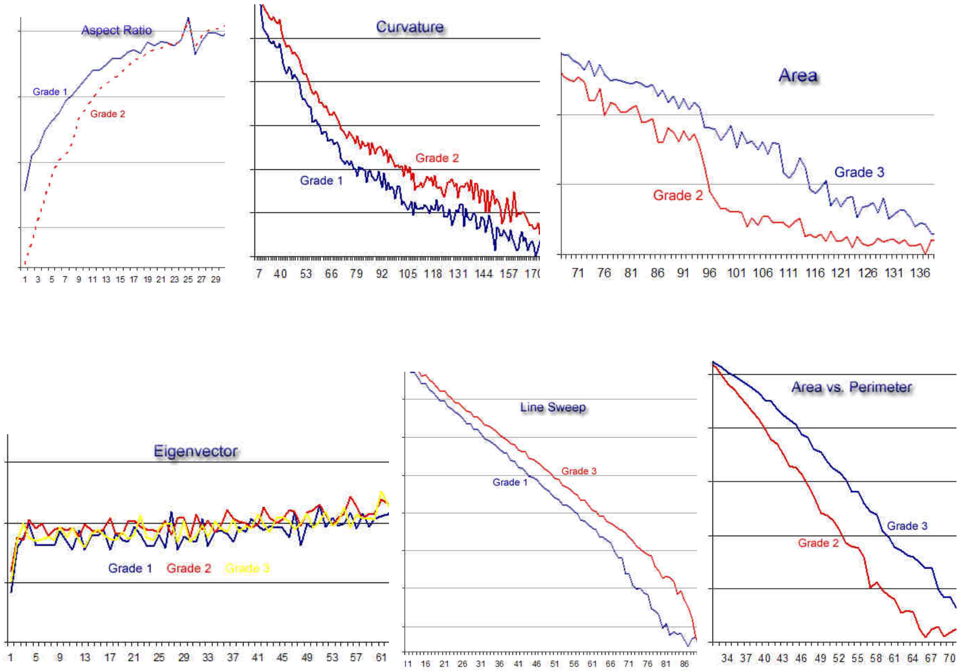

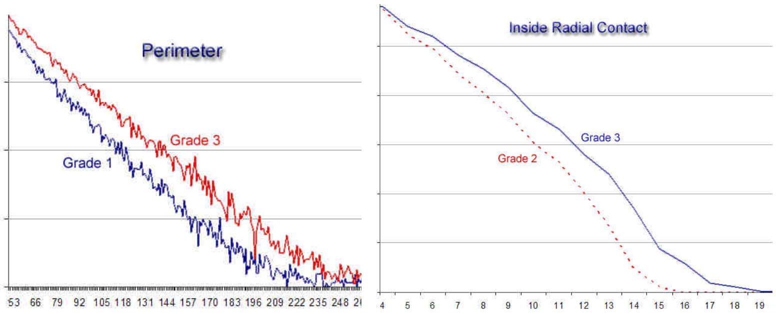

Figure 4-1 Regions of good separations

It should also be kept in mind that if a sub-region gets too small it will not be able to capture enough information about the image. Though this is domain and metric specific, we assume that if the sub-region shrinks below 40% it will start to become an inaccurate/incomplete description of the image. Though sub-regions might seem to be a good estimation, it should not be a replacement for comparing the whole histogram after filtering out the sparse regions.

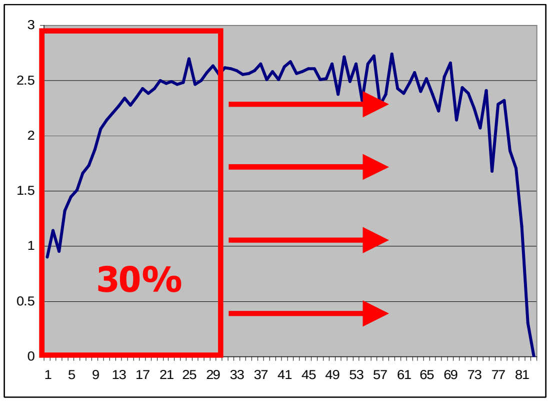

Figure 4-2 Sub-region sliding window

4.3 Information retrieval analysis

The final stage of this whole process is to analyze the relative success of our shape distributions and to do that we chose to use information retrieval methods. Due to the consideration for the sub-regions of good separation we have decided to analyze all sub-regions within the final trimmed window of all histograms for each shape measure. We performed this by sweeping a sliding window (Figure 4-2) over the cropped regions with a given window size by incrementing the starting location of the window one bucket location at a time. The window size has been described earlier as 50% to 100% in increments of 10%. Each geometric measure will have every possible window in the cropped regions analyzed by the sliding window at every window size.

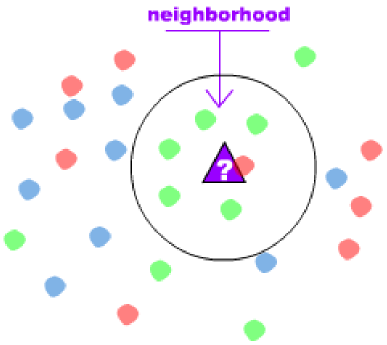

Figure 4-3 K nearest neighbor

We would then perform EMD calculations for all the sub-region of the same window size against each other and attempt to validate our known histological grades associated with each case based on a K-nearest-neighbor query. K-nearest-neighbor takes a set of data points and using some form of edit distance finds the K closest points around an unknown point (Figure 4-3). So in our case of analyzing the performance of a given sub-regions in a given geometric measure we would, for all cases, find the K nearest cases to a given case based on EMD distance and try to form a result for our K-nearest-neighbor query based on a vote between all K nearest cases. The final result of the query would be the histological grade with the highest vote [11] [17]. If there is a tie in the vote, the given case would be classified as "unknown".

The K values that we chose for the classification process are 4, 7, and 10. We chose these values in order to guarantee that only a two way tie is possible if a tie exists, eliminating the possibility of three way ties, as shown by K **mod** 3 producing 1 for each K value. We chose to omit the K value of 1 from our analysis because we observe that it wouldn't be any different from just getting the closest case, providing an unreliable classification. We did not go above 10 for the K value because we only have ten cases for each grade, providing us with no meaningful information.

The next step that we took was to take the queries of each sub-region of each geometric measure formed by K nearest neighbor and analyzing them using the metrics of precision, recall and F-measure. As a precursor, we should define the following terms [48]:

- True Positive (TP): In a given set of cases with known classification, how many cases were correctly classified into class X by a classifier.

- False Positive (FP): In the same set of cases, how many cases that don’t belong in class X were classified into class X by the classifier.

- False Negative (FN): In the same set of cases, how many cases that belong in class X did not make it into class X.

Precision measure how many correct queries were performed for each histological grade in respect to all the queries that maps a case to that specific histological grade. The precision of K nearest neighbor in histological grade C_j is generated by taking the sum of all correct queries (true positives, TP) and dividing it by the total number of queries performed (true positives + false positives, TP + FP) (Equation 4-1). The goal of each window is to maximize precision [48].

$$Precision\left(C_j\right) = \frac{TP}{TP + FP}$$

Equation 4-1 Precision measure

The recall metric measures how many cases of a certain histological grade were able to get mapped back to their original classification using a query. Recall is the ratio between the correct queries for the histological grade (TP) and all the cases that belong to the histological grade (TP + FN). The goal of each window is to maximize recall [48].

$$Recall\left(C_j\right) = \frac{TP}{TP + FN}$$

Equation 4-2 Recall measure

The F-measure is a metric that combines both precision and recall in a harmonic mean (geometric mean squared over arithmetic mean) to provide an overall performance measure that combines both individual measures (Equation 4-3). The scale of the F-measure is from 0.0 to 1.0. Almost 0.0 is the worst performance and 1.0 is best [48] [35].

$$F\left(C_j\right) = \frac{2 \times precision \times recall}{precision + recall}$$

Equation 4-3 F-measure

The full process of analyzing each window will consist of computing precision, recall and F-measure for each window. Analysis for each window will be stored and ranked using F-measure as key. A summary of the best performance, in respect F-measure, can be found in Appendix A. The metric for best performance is ranked primarily by F-measure and if there is a tie with the F-measure it will be ranked secondarily by window size second. A visualization of this data can be seen below with Figure 4-4, Figure 4-6 and Figure 4-8 and descriptions. The full set of data for our images acquired from this process can be found in the link in Appendix B.

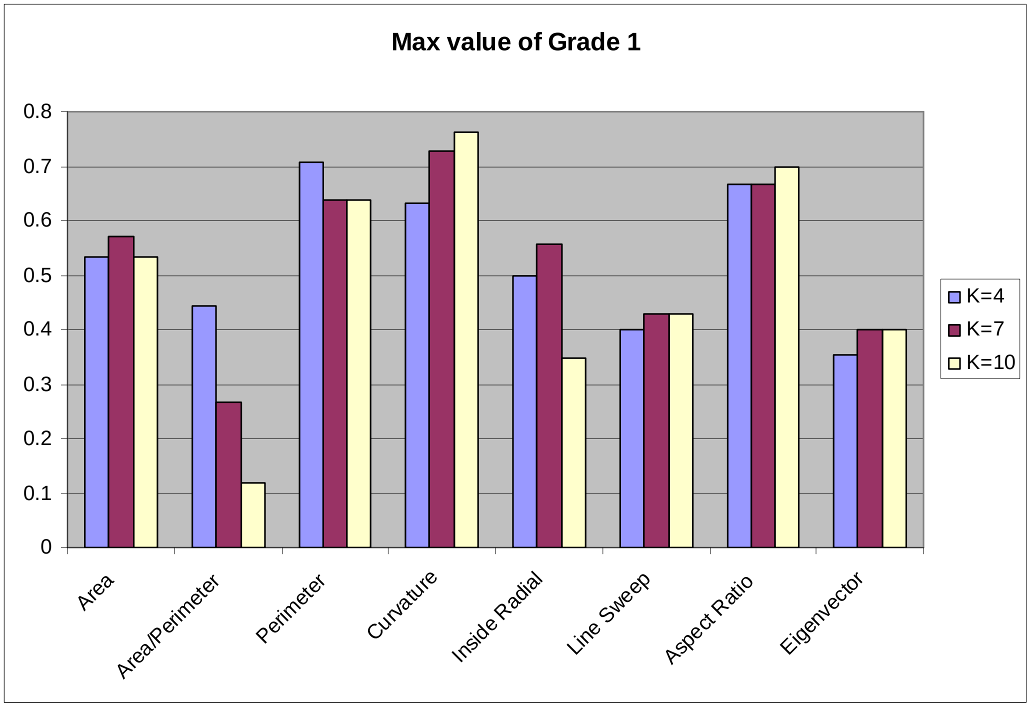

Figure 4-4 Maximum performance value of
Grade 1 in respect to k-values.

The grade 1 analysis shows that curvature came out with the best F-measure of all the geometric measures. From Figure 4-4 we can see that curvature performs better, in respect to F-measure, with higher K value in the K-nearest-neighbor query. The second best window for grade 1 is perimeter and contrary to curvature it performs better with a lower K value of 4. The third best window in grade 1 is aspect ratio, which performed similar across all K values. The details of the three best windows in grade 1 can be viewed in Table 4-1.

Table 4-1 Best performing windows for Grade 1

Metric	Window	Precision	Recall	F-measure
Curvature	Window 103 to 207 (60%)	8/11	8/10	0.7619
Perimeter	Window 17 to 162 (60%)	6/7	6/10	0.7059
Aspect Ratio	Window 11 to 51 (50%)	7/10	7/10	0.7

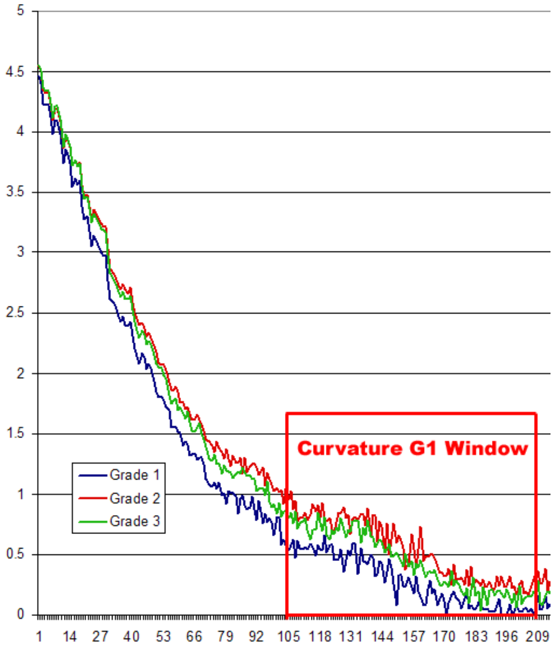

Figure 4-5 Grade 1 best window

Upon visual inspection of the best performing window in grade 1 in Figure 4-5, it is visible that the window did pick up the region of best separation. The graph shows the average histograms for grade 1, 2 and 3 with the noisy tail trimmed.

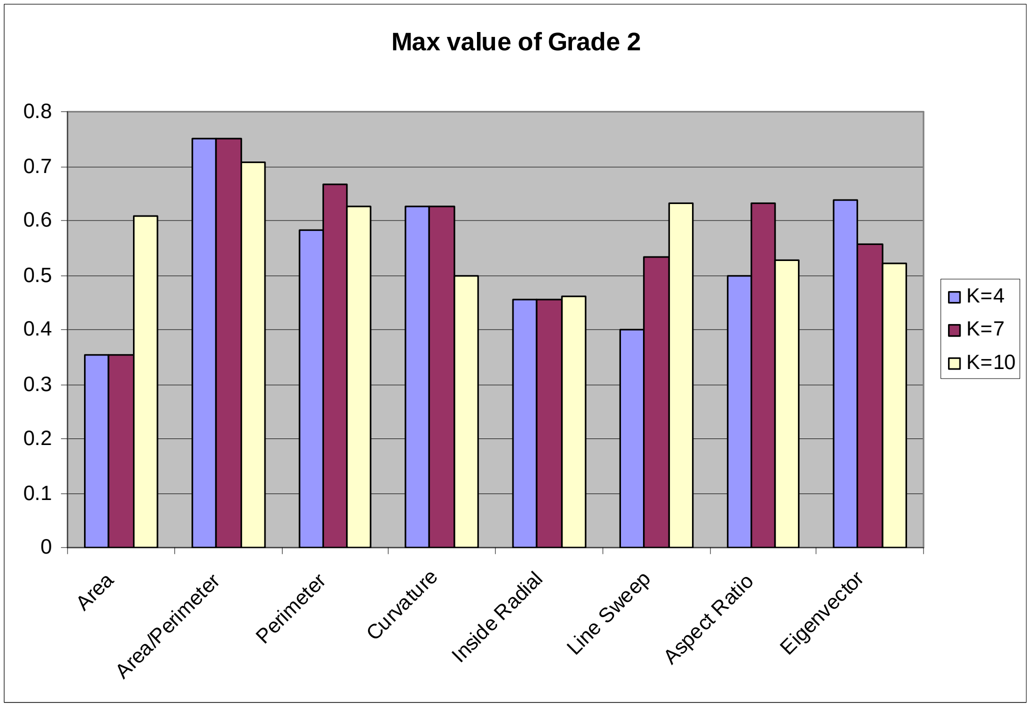

Figure 4-6 Maximum performance value of
Grade 2 in respect to k-values.

The grade 2 analysis in Figure 4-6 shows area vs. perimeter to have the best window in respect to F-measure performance. For grade 2, area vs. perimeter showed good performance with K values of both 4 and 7. The second best measure for grade 2 is perimeter. Perimeter seems to peek in performance with a K value of 7. It is interesting to note that area vs. perimeter came out with a better score than area or perimeter alone, showing that there isn't a direct correlation between the three measures with regards to the final result. The third best measure for grade 2 is eigenvector. Eigenvector seems to do better with lower K values with the best performance coming from K value of 4. This almost validates our observation earlier stating that eigenvector seems to have a very chaotic behavior when inspected visually. It seems to have many localized oscillations that all tend towards a common trend, regardless of the histological grade. As our full data set (Appendix B) will show, eigenvector has pockets of windows of good performance within the sliding window analysis. The graph in Figure 4-6 verifies that it performs better with less information. The details of the three best windows in grade 2 can be viewed in Table 4-2.

Table 4-2 Best performing windows for Grade 2

Metric	Window	Precision	Recall	F-measure
Area / Perimeter	Window 43 to 82 (60%)	6/6	6/10	0.75
Perimeter	Window 31 to 152 (50%)	6/8	6/10	0.6667
Eigenvector	Window 33 to 63 (50%)	7/12	7/10	0.6364

A closer visual inspection of the best window in grade 2 in Figure 4-7 shows that it is actually debatable whether the sub-region is a region of good separation. It shows the window to be a good sub-region for grade 3 but not visibly so for grade 2. What we suspect the analysis to have done is that it takes the average separation of grade 2 from grade 1 and grade 2 and determines the performance based on that. From Table 4-2 we can see that only six cases were accurately queried from grade 2, which is about half of the original ten cases that were identified as grade 2. From speaking with our pathologist, he suggests that this could also be due to the ambiguity of classifying a case as grade 2, even for humans.

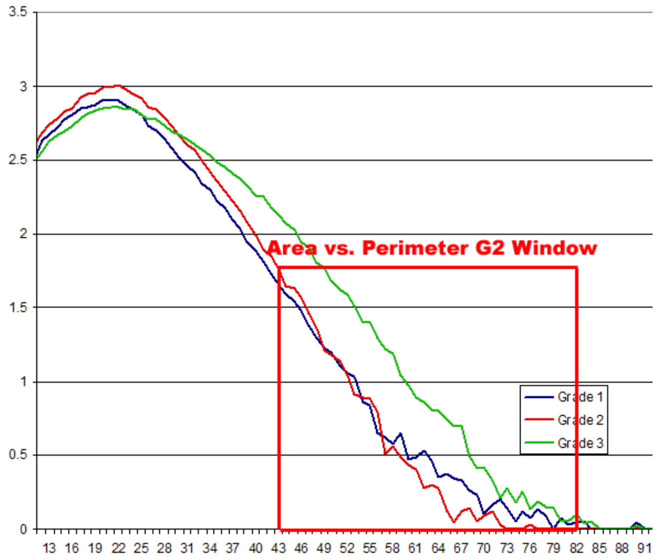

Figure 4-7 Grade 2 best window

The grade 3 analysis in Figure 4-8 shows inside radial contact to be the geometric measure with the best window for grade 3. Inside radial contact shows that it performs better with higher K value. The second best measure for grade 3 in regards to F-measure is curvature. Curvature, for grade 3, performs better with lower K value, though it shows no overall trend for how K value affects performance. The third best measure for grade 3 is aspect ratio. Aspect ratio peeks in performance with a K value of 7. The details of the three best windows in grade 3 can be viewed in Table 4-3.

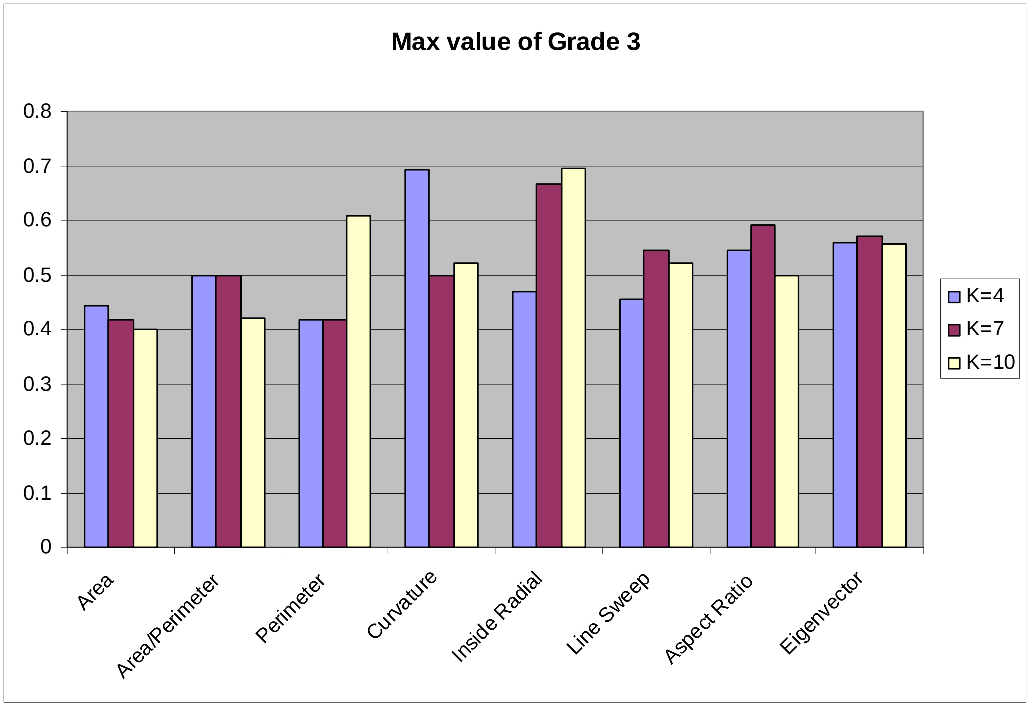

Figure 4-8 Maximum performance value of Grade 3 in respect to k-values.

Table 4-3 Best performing windows for Grade 3

Metric	Window	Precision	Recall	F-measure
Inside Radial Contact	Window 8 to 20 (60%)	8/12	8/11	0.6957
Curvature	Window 48 to 152 (60%)	9/15	9/11	0.6923
Aspect Ratio	Window 33 to 78 (70%)	8/16	8/11	0.5926

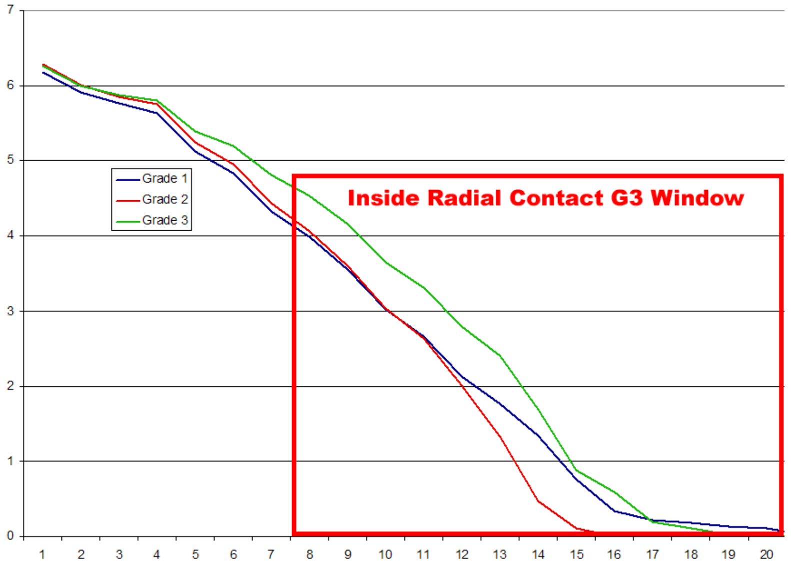

Figure 4-9 Grade 3 best window

From visually inspecting the best performing window in grade 3 in Figure 4-9 we can see that it is obvious that the window picked out the sub-region of best separation. It clearly distinguishes the grade 3 average histogram from the other two grades within the region. Though it is not as clear at the tail of the histogram, it is the best sub-region of separation between bucket locations of 8 and 13.

Chapter 5

CONCLUSION

5.1 Conclusion

This thesis has investigated the use of shape distributions in the analysis of segmentations of histological images. From our studies we have discovered a way to analyze the performance of shape distributions based on their ability to estimate histological grade. We explored the feasibility and performance of the Earth Mover's Distance as an edit distance in our analysis. While our results are suggestive of predictions using visual and quantitative methods, they are not predictive at this point. What we have shown is a quantitative technique for determining best windows of predictive results for each metric and K-value when using the K-nearest-neighbor method, regardless of the techniques and edit distances used.

Besides the analysis of shape distributions for histological segmentations we were also able to explore the extension of using a line as a shape function. Using the line sweep shape function we were able to emulate the profile shape function [47] and take it further by collecting all possible profiles of the image.

5.2 Future work

Though this approach offers good start, there is more that can be done to improve it. One of the major improvements that could be implemented is the incorporation of multi-level magnification. We propose to apply a Gaussian pyramid approach to help add the ability to zoom out of the image. It would also be useful to have images of very high magnification to start with when working with such scheme. Many of the metrics would benefit greatly from added details in the image, as well as a more zoomed out view.

This work can be improved if other classification techniques and edit distances are explored. This can lead to measuring and comparing the relative quality of each technique and edit distance in relationship to the data given. We would also like to determine if shape distributions may be improved with other techniques and edit distances.

Our study would have benefited from more histological segmentations for analysis. This would provide more statistical information. More data would allow us to move closer to a predictive capability. With enough evidence we could possibly calculate a statistical likelihood of a certain case being a certain grade.

With enough data and evidence we would eventually want this work to be validated for image archiving and cataloging purposes. This work can easily be ported over for image archiving and cataloging and we wish fully explore this at a later time.

Appendix A

BEST PERFORMANCE

This appendix lays out all the best windows, in respect to F-measure, of each geometric measure. For more information on each measurement please consult chapter 4.3.

Area

K=4

Grade	Window	Precision	Recall	F-measure
Grade 1	Window 2 to 98 (70%)	4/5	4/10	0.533
Grade 2	Window 0 to 69 (50%)	3/7	3/10	0.353
Grade 3	Window 5 to 101 (70%)	4/7	4/11	0.444

K=7

Grade	Window	Precision	Recall	F-measure
Grade 1	Window 46 to 128 (60%)	4/4	4/10	0.571
Grade 2	Window 11 to 80 (50%)	5/9	5/10	0.526
Grade 3	Window 5 to 101 (50%)	5/13	5/11	0.417

K=10

Grade	Window	Precision	Recall	F-measure
Grade 1	Window 9 to 105 (70%)	4/5	4/10	0.533
Grade 2	Window 64 to 133 (50%)	7/13	7/10	0.609
Grade 3	Window 18 to 87 (50%)	4/9	4/11	0.4

Area vs. Perimeter

K=4

Grade	Window	Precision	Recall	F-measure
Grade 1	Window 5 to 68 (80%)	4/8	4/10	0.444
Grade 2	Window 44 to 83 (50%)	6/6	6/10	0.75
Grade 3	Window 22 to 69 (60%)	4/5	4/11	0.5

K=7

Grade	Window	Precision	Recall	F-measure
Grade 1	Window 7 to 78 (90%)	2/5	2/10	0.267
Grade 2	Window 43 to 82 (50%)	6/6	6/10	0.75
Grade 3	Window 7 to 46 (50%)	6/13	6/11	0.5

K=10

Grade	Window	Precision	Recall	F-measure
Grade 1	Window 5 to 44 (50%)	2/8	2/10	0.222
Grade 2	Window 15 to 62 (60%)	6/7	6/10	0.706
Grade 3	Window 7 to 70 (80%)	4/8	4/11	0.421

Curvature

K=4

Grade	Window	Precision	Recall	F-measure
Grade 1	Window 76 to 201 (60%)	6/9	6/10	0.632
Grade 2	Window 89 to 193 (50%)	5/6	5/10	0.625
Grade 3	Window 48 to 152 (50%)	9/15	9/11	0.692

K=7

Grade	Window	Precision	Recall	F-measure
Grade 1	Window 82 to 207 (60%)	8/12	8/10	0.727
Grade 2	Window 52 to 156 (50%)	5/6	5/10	0.625
Grade 3	Window 23 to 127 (50%)	6/13	6/11	0.5

K=10

Grade	Window	Precision	Recall	F-measure
Grade 1	Window 103 to 207 (50%)	8/11	8/10	0.762
Grade 2	Window 86 to 190 (50%)	4/6	4/10	0.5
Grade 3	Window 25 to 129 (50%)	6/12	6/11	0.522

Eigenvector

K=4

Grade	Window	Precision	Recall	F-measure
Grade 1	Window 52 to 77 (50%)	3/7	3/10	0.353
Grade 2	Window 33 to 63 (60%)	7/12	7/10	0.636
Grade 3	Window 49 to 74 (50%)	7/14	7/11	0.56

K=7

Grade	Window	Precision	Recall	F-measure
Grade 1	Window 33 to 63 (60%)	3/5	3/10	0.4
Grade 2	Window 44 to 79 (70%)	5/8	5/10	0.556
Grade 3	Window 38 to 78 (80%)	6/10	6/11	0.571

K=10

Grade	Window	Precision	Recall	F-measure
Grade 1	Window 33 to 63 (60%)	3/5	3/10	0.4
Grade 2	Window 37 to 67 (60%)	6/13	6/10	0.522
Grade 3	Window 48 to 78 (60%)	5/7	5/11	0.556

Inside Radial

K=4

Grade	Window	Precision	Recall	F-measure
Grade 1	Window 8 to 20 (60%)	4/6	4/10	0.5
Grade 2	Window 4 to 14 (50%)	5/12	5/10	0.455
Grade 3	Window 6 to 18 (60%)	4/6	4/11	0.471

K=7

Grade	Window	Precision	Recall	F-measure
Grade 1	Window 10 to 20 (50%)	5/8	5/10	0.556
Grade 2	Window 43 to 82 (60%)	5/12	5/10	0.455
Grade 3	Window 1 to 13 (50%)	7/10	7/11	0.667

K=10

Grade	Window	Precision	Recall	F-measure
Grade 1	Window 10 to 20 (50%)	4/13	4/10	0.348
Grade 2	Window 0 to 12 (60%)	6/16	6/10	0.462
Grade 3	Window 8 to 20 (60%)	8/12	8/11	0.696

Line Sweep

K=4

Grade	Window	Precision	Recall	F-measure
Grade 1	Window 10 to 103 (70%)	4/10	4/10	0.4
Grade 2	Window 22 to 88 (50%)	4/10	4/10	0.4
Grade 3	Window 13 to 119 (80%)	5/11	5/11	0.455

K=7

Grade	Window	Precision	Recall	F-measure
Grade 1	Window 6 to 85 (60%)	3/4	3/10	0.429
Grade 2	Window 14 to 80 (50%)	4/5	4/10	0.533
Grade 3	Window 8 to 101 (70%)	6/11	6/11	0.546

K=10

Grade	Window	Precision	Recall	F-measure
Grade 1	Window 21 to 87 (50%)	3/4	3/10	0.429
Grade 2	Window 19 to 85 (50%)	6/9	6/10	0.632
Grade 3	Window 26 to 119 (70%)	6/12	6/11	0.522

Major/Minor Axis

K=4

Grade	Window	Precision	Recall	F-measure
Grade 1	Window 10 to 47 (50%)	6/8	6/10	0.667
Grade 2	Window 21 to 58 (50%)	4/6	4/10	0.5
Grade 3	Window 10 to 77 (90%)	6/11	6/11	0.546

K=7

Grade	Window	Precision	Recall	F-measure
Grade 1	Window 12 to 57 (60%)	6/8	6/10	0.667
Grade 2	Window 19 to 85 (80%)	6/9	6/10	0.632
Grade 3	Window 33 to 78 (60%)	8/16	8/11	0.593

K=10

Grade	Window	Precision	Recall	F-measure
Grade 1	Window 14 to 51 (50%)	7/10	3/10	0.7
Grade 2	Window 27 to 64 (50%)	5/9	5/10	0.526
Grade 3	Window 19 to 79 (80%)	7/17	7/11	0.5

Perimeter

K=4

Grade	Window	Precision	Recall	F-measure
Grade 1	Window 17 to 162 (60%)	6/7	6/10	0.706
Grade 2	Window 96 to 241 (60%)	7/14	7/10	0.583
Grade 3	Window 73 to 218 (60%)	5/13	5/11	0.417

K=7

Grade	Window	Precision	Recall	F-measure
Grade 1	Window 55 to 224 (70%)	7/12	7/10	0.636
Grade 2	Window 84 to 205 (50%)	7/11	7/10	0.667
Grade 3	Window 36 to 205 (70%)	5/13	5/11	0.417

K=10

Grade	Window	Precision	Recall	F-measure
Grade 1	Window 53 to 222 (70%)	7/13	7/10	0.636
Grade 2	Window 34 to 203 (70%)	5/6	5/10	0.625
Grade 3	Window 12 to 157 (60%)	7/12	7/11	0.609

Appendix B

ONLINE RESOURCES

For all data pertaining to all experiments please visit:

http://www.cs.drexel.edu/~jzz22/thesis . If any concerns regarding this thesis may arise, please contact me at jzz22@drexel.edu.

LIST OF REFERENCES

1. J. Aßfalg, K. M. Borgwardt, H. Kriegel, 3DString: a feature string kernel for 3D object classification on voxelized data. *Proceedings of the 15th ACM international Conference on information and Knowledge Management*, 2006

2. P. H. Bartels, G.L. Wied, Computer analysis and biomedical interpretation of microscopic images: Current problems and future directions, *Proceedings of the IEEE* , vol.65, no.2, pp. 252-261, 1977

3. Spotting medical mistakes, *BBC News*, June 13, 2000

4. G. Borgefors, Distance transformations in arbitrary dimensions, *Computer Vision, Graphics, and Image Processing,* vol. 27, pp. 321-345, 1984

5. D. Breen, R. Fedkiw, K. Museth, S. Osher, G. Sapiro, R. Whitaker, Level set and PDE methods for computer graphics. *ACM SIGGRAPH 2004 Course Notes*, 2004

6. J. E. Bresenham, Algorithm for computer control of a digital plotter, *IBM Systems Journal*, vol. 4, 1, 1965

7. I. Carlbom, I. Chakravarty, W. M. Hsu. SIGGRAPH'91 Workshop Report Integrating Computer Graphics, Computer Vision, and Image Processing in Scientific Applications, *ACM SIG GRAPH Computer Graphics*, Volume 26, Issue 1, 1992)

8. K. R. Castleman, *Digtal Image Processing*, Prentice Hall, 1996

9. C. Chambers, D. Ungar, Making pure object-oriented languages practical. *Conference Proceedings on Object-Oriented Programming Systems, Languages, and Applications*, 1991

10. S. J. Colley, *Vector Calculus*, Prentice Hall, 2nd edition, 2002

11. L. F. Costa, R. M. Cesar Jr. *Shape Analysis and Classification: Theory and Practice*, CRC, 2000

12. W. J. Dally, J. T. Kajiya, An object oriented architecture. *Proceedings of the 12th Annual international Symposium on Computer Architecture*, 1985

13. P. E. Danielsson, Euclidean distance mapping, *CVGIP*, vol. 14, pp. 227-248, 1980

14. M. Datar, D. Padfield, H. Cline. Color and Texture Based Segmentation of Molecular Pathology Images using HSOMs, *Proceedings of 2nd Workshop on Microsopic Image Analysis with Applications in Biology*, 2007

15. J. L. Devore, *Probability and Statistics for Engineering and the Scien*ces, Duxbury Press, 7th edition, 2007

16. S. Doyle, M. Hwang, K. Shah, A. Madabhushi, J. Tomasezweski, M. Feldman, Automated Grading of Prostate Cancer using Architectural and Textural Image Features, *International Symposium on Biomedical Imaging*, pp. 1284-87, 2007

17. R. O. Duda, P. E. Hart, D. G. Stork, *Pattern Classification*, Wiley-Intersience; 2nd edition, 2001

18. A. Elinson, D. S. Nau, W. C. Regli, Feature-based similarity assessment of solid models. In *Proceedings of the Fourth ACM Symposium on Solid Modeling and Applications*, 1997

19. D. Freedman, T. Zhang, Interactive graph cut based segmentation with shape priors, *Computer Vision and Pattern Recognition, 2005. CVPR 2005. IEEE Computer Society Conference on* , vol.1, no., pp. 755-762 vol. 1, 20-25 June 2005

20. T. Funkhouser, P. Min, M. Kazhdan, J. Chen, A. Halderman, D. Dobkin, D. Jacobs, A search engine for 3D models. *ACM Trans. Graph.* vol. 22, 1, 2003

21. G. Golub and C. van Loan. *Matrix Computations*, The Johns Hopkins University Press; 3rd edition, 1996

22. R. C. Gonzalez, R. E. Woods, S. L. Eddins. *Digital Image Processing with Matlab*, Prentice Hall, 2004

23. S. K. Gupta, W. C. Regli, D. S. Nau, Manufacturing feature instances: which ones to recognize?. *Proceedings of the Third ACM Symposium on Solid Modeling and Applications*, 1995

24. R. Haralick and L. Shapiro *Computer and Robot Vision*, Vol. 1, Chap. 5, Addison-Wesley Publishing Company, 1992

25. U. Hölzle, D. Ungar, Reconciling responsiveness with performance in pure object-oriented languages. *ACM Trans. Program. Lang. Syst.*, 1996

26. B. K. P. Horn, *Robot Vision*, The MIT Press, 1986

27. M. H. Hueckel, A Local Visual Operator Which Recognizes Edges and Lines. *Journal of the ACM* 20, 1973

28. 2007. Insight Toolkit (ITK).
http://www.itk.org

29. C. Ip and D. Lapadat and L. Sieger and W. Regli. Using shape distributions to compare solid models, *In Seventh ACM Symposium on Solid Modeling and Applications.* ACM SIGGRAPH, ACM Press, Jun 17-23 2002.

30. A. Jain. *Fundamentals of Digital Image Processing*, Prentice-Hall, 1989

31. R. Jain and Y. Roth. Visualization and computer vision. *Position paper for the SIGGRAPH'91 Workshop on Integrating Computer Graphics, Computer Vision, and hnage Processing in Scientific Applications*, 1991.

32. K. J. Khouzani, H. Soltanian-Zadeh, Automatic grading of pathological images of prostate using multiwavelet transform, *Engineering in Medicine and Biology Society, 2001. Proceedings of the 23rd Annual International Conference of the IEEE*, 2545 - 2548 vol.3, 2001

33. H. M. Ladak, F. Mao; Y. Wang; D. B. Downey, D. A. Steinman, A. Fenster, Prostate segmentation from 2D ultrasound images, *Engineering in Medicine and Biology Society, 2000. Proceedings of the 22nd Annual International Conference of the IEEE*, vol.4, pp.3188-3191, 2000

34. F. M. Lopes,. L. A.. Consularo, A RBFN Perceptive Model for Image Thresholding, *Computer Graphics and Image Processing, 2005. SIBGRAPI 2005. 18th Brazilian Symposium on* , pp. 225-232, 2005

35. J. Makhoul, F. Kubala, R. Schwartz, R. Weischedel, Performance measures for information extraction. *Proceedings of DARPA Broadcast News Workshop*, 1999

36. M. Masseroli, S. Bonacina, F. Pinciroli, Java-Based Browsing, Visualization and Processing of Heterogeneous Medical Data from Remote Repositories," *Engineering in Medicine and Biology Society, 2004. IEMBS '04. 26th Annual International Conference of the IEEE* , vol.2, pp. 3326-3329, 2004

37. K. Minho, H. Yo-Sung, Semi-automatic segmentation by a double labeling method, *TENCON 99. Proceedings of the IEEE Region 10 Conference* , vol.1, pp.746-749, 1999

38. E. N. Mortensen, J. Jia, Real-Time Semi-Automatic Segmentation Using a Bayesian Network, *Computer Vision and Pattern Recognition, 2006 IEEE Computer Society Conference on* , vol.1, pp. 1007-1014, 2006

39. D. Mumford, J. Shah. Optimal approximations by piecewise smooth functions and associated variational problems, *Communications on Pure and Applied Mathematics, Vol. XLII*, pp 577-685, 1989

40. S. Naik, S. Doyle, M. Feldman, J. Tomaszewski, A. Madabhushi, Gland Segmentation and Gleason Grading of Prostate Histology by Integrating Low-, High-level and Domain Specific Information, *Proceedings of 2nd Workshop on Microsopic Image Analysis with Applications in Biology*, 2007

41. K. Nandy, P.R. Gudla, S.J. Lockett. Automatic Segmentation of Cell Nuclei in 2D Using Dynamic Programming, *Proceedings of 2nd Workshop on Microsopic Image Analysis with Applications in Biology*, 2007

42. R. Osada, T. Funkhouser, B. Chazelle, D. Dobkin, Shape distributions. *ACM Transaction on Graphics*, vol. 21, 4, pp. 807-832, 2002

43. J. L. Pajon, V. Bui-Tran, and C. Bennis. Scientific visualization: A way of reconciling experimentation and modeling. *Position paper for the SIGGRAPH'91 Workshop on Integrating Computer Graphics, Computer Vision, and Image Processing in Scientific Applications*, 1991.

44. M. Peabody, *Finding Groups of Graphs in Databases*, Master's Thesis, Drexel University, 2002

45. S. Petushi, C. Katsinis, C. Coward, F. Garcia, A. Tozeren, Automated identification of microstructures on histology slides, *Biomedical Imaging: Nano to Macro, 2004. IEEE International Symposium on* , pp. 424-427 Vol. 1, 2004

46. S. Petushi, J. Marker, J. Zhang, W. Zhu, D. Breen, C. Chen, X. Lin, F.Garcia, A Visual Analytics System for Breast Tumor Evaluation, *Analytical and Quantitative Cytology and Histology* , 2007

47. W. C. Regli, D. S. Nau, Building a general approach to feature recognition of Material Removal Shape Element Volumes (MRSEVs), *Proceedings on the Second ACM Symposium on Solid Modeling and Applications*, 1993

48. C. J. van Rijsbergen, *Information Retrieval*, Butterworth-Heinemann; 2Rev Ed edition, March 1979

49. A. Rosenfeld, J. Pfaltz, *Distance Functions in Digital Pictures*, Pattern Recognition, Vol 1, pp 33-61, 1968

50. Y. Rubner, C. Tomasi. *Perceptual Metrics for Image Database Navigation.* Kluwer Academic Publishers, Boston, December 2000

51. Y. Rubner, C. Tomasi, L. J. Guibas. The Earth Mover's Distance as a Metric for Image Retrieval, *International Journal of Computer Vision 40(2),* 99–121, 2000

52. J. A. Sethian. *Level Set Methods and Fast Marching Methods*, Cambridge University Press; 2nd edition, 1999

53. N. L. Sizto, L. J. Dietz, *Method and apparatus for cell counting and cell classification*, US Patent: 5556764, 1994

54. G. Smith. Pathologist shortage hits small towns hard, *Chicago Tribune*, Oct. 11, 2007

55. G. Strang, *Introduction to Linear Algebra*, Wellesley-Cambridge, 2003

56. A. Verma, A. Kriete, Robust Object-Oriented Segmentation for High-Content Screening, *Proceedings of 2nd Workshop on Microsopic Image Analysis with Applications in Biology*, 2007

57. A. R. Weeks, *Fundamentals of Electronic Image Processing*, Wiley-IEEE Press, 1996

58. G. Winkler, *Image Analysis, Random Fields and Markov Chain Monte Carlo Methods: A Mathematical Introduction*, Springer-Verlag; 2nd edition, 2003